表面プラズモン共鳴法によるPrP^Cとの相互作用を利用したスクリーニング法[8]が新たに開発されている．

高感度プリオン検出法の開発

PrP^{Sc}の検出法には，プロテアーゼ処理によって混在するPrP^Cを除去し，プロテアーゼ耐性のPrP^{Sc}をメンブレンあるいはプレート上で免疫化学的に測定するウェスタンブロット法やELISA法が従来使用されてきた．その後，PrP^{Sc}に特異性を持つポリマーでコーティングしたプレートを用いるELISA法や，コンフォメーションを認識する抗体を用いたELISA法(CDI法)[9]など，プロテアーゼ処理を省略した検出法も開発されている．また，PrP^{Sc}との相互作用によってコンフォメーション変化を起こし，蛍光を発するよう工夫されたペプチドを用いた高感度検出法や，DNAの増幅に使われているPCR法によく似た原理によって*in vitro*でPrP^{Sc}を増幅するという検出法(PMCA法)[10]など，新しい原理による検出法も開発されている．PMCA法は，PrP^{Sc}からなる凝集体がある条件下でPrP^Cを重合して，より大きなPrP^{Sc}凝集体を形成することを利用している．一定時間ごとに超音波処理と重合反応を繰り返すことによりPrP^{Sc}を増幅するという方法で，これまで最も感度の良かったバイオアッセイをしのぐ感度を有しており，ごく低濃度のPrP^{Sc}の検出などにおいて，現在最も高感度の測定法となっている．現在のところ，増幅できるプリオンは限定されるなど，まだ克服すべき点があるが，反応の自動化も完了しており，血液や尿など低濃度のプリオンを含む試料の高感度検出とプリオン病の早期発見への応用に期待されている．

プリオン病の治療薬候補

プリオン病の治療薬候補として，多くの薬剤，化合物が報告されている．最近になって，さまざまなアッセイ系によってこれまでスクリーニングされたプリオン病予防薬・治療薬について体系的に検討された結果が，Brain誌に報告されている[11]ので参照されたい．

①アミロイド結合性を持つCongo red[11]，

②抗アミロイド活性を持つ抗癌剤ヨードドキソルビシン(4'-deoxy-4'-iododoxorubicin；IDOX)[12]とその構造類似体のテトラサイクリン(tetracycline)[13]，

③抗ウイルス薬からスクリーニングによって見出されたアンフォテリシンB(amphotericin B；AmB)[14]などのポリエン系抗生物質，

④アミロイド結合性を持つペントサンポリサルフェート(pentosan polysulfate；PPS)[15]などのポリアニオン誘導体，

⑤アミロイドなどのβシート構造を破壊するペプチド[16]，

⑥蛋白質と結合し，立体構造に変化を与えるポルフィリン(porphyrin)などのテトラピロール類[17]，

⑦特定の構造を持つトランスフェクシ

表1　プリオン病治療薬候補

プリオン病治療薬候補化合物	化合物名	発見の経緯，化合物の特徴
アミロイド結合性化合物	Congo red	アミロイド結合性
四環系化合物	IDOX，テトラサイクリン	抗癌剤，抗アミロイド活性
ポリエン系抗生物質	アンフォテリシンB	抗ウイルス薬よりスクリーニング
ポリアニオン系化合物	ペントサンポリサルフェート	同上
βシート破壊ペプチド	iPrP13	アミロイド構造の破壊
テトラピロール系化合物	FeTSP	蛋白質構造変化促進，Congo red様構造
ポリアミン化合物	PAMAM	トランスフェクション試薬，抗プリオン作用
三環系化合物	キナクリン，クロルプロマジン	抗マラリア薬，抗精神病薬，BBB透過
抗体，免疫賦活剤	抗PrP抗体6H4，D18	PrP^Cへの結合
その他	メマンチン，フルピルチン	NMDA受容体アゴニスト，抗神経細胞死

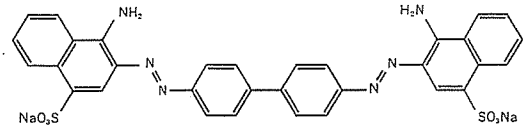

Congo red

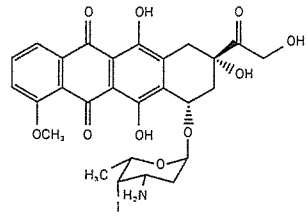

ヨードドキソルビシン

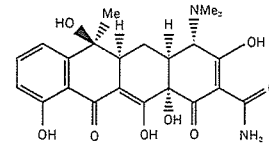

テトラサイクリン

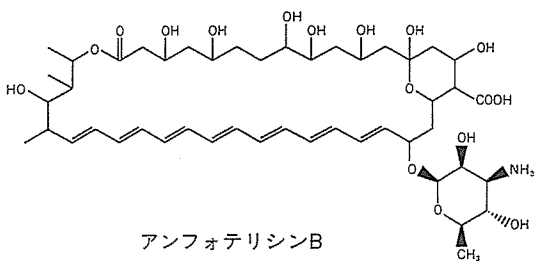

アンフォテリシンB

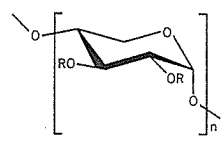

ペントサンポリサルフェート
(R＝SO_3Na，n＝12)

PrP　^{115}A　AA AG AV V^{122}

iPrP13　DAPAAPAGPAVPV

β シート破壊ペプチド

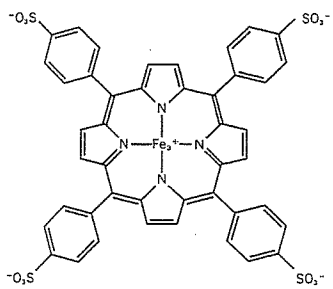

FeTSP
Iron(Ⅲ)meso-tetra(4-sulphonatophenyl)Porphine

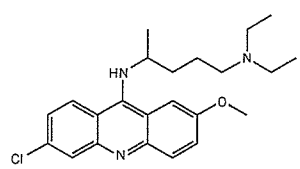

キナクリン

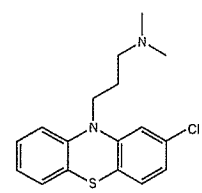

クロルプロマジン

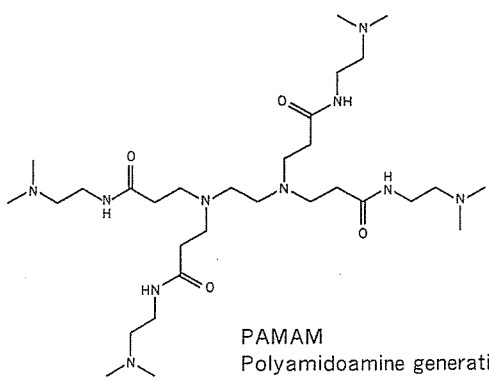

PAMAM
Polyamidoamine generation 0

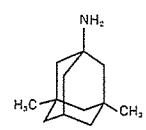

メマンチン

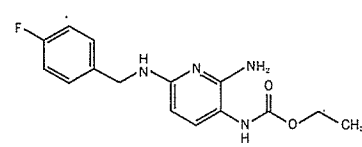

フルピルチン

図1　さまざまなプリオン病治療薬

ョン試薬が抗プリオン活性を示すことから見出された分岐性ポリアミン，
⑧抗プリオン蛋白抗体[10]，
⑨血液脳関門(BBB)を透過する既存の治療薬からスクリーニングにより見つかった抗マラリア薬キナクリン(quinacrine)[18]や抗精神薬クロルプロマジン(chlorpromazine)[19]など，
⑩神経細胞死を抑制する薬剤からNMDA受容体拮抗薬メマンチン(memantine)[20]や中枢性鎮痛薬フルピルチン(flupirtine)[20]，
などがある(表1，図1)．これらのなかで，実際に患者に応用されている薬剤および化合物には，AmB，PPS，キナクリン，フルピルチンなどがある．本稿では，キナクリン，PPSおよびフルピルチンについて解説する．

キナクリンは，長年にわたって抗マラリア薬として広く使用されてきた薬剤であり，安全性も高いことから，米国，フランス，英国などにて臨床研究が進められている．わが国においても孤発性CJD 22例，医原性CJD 5例，遺伝性プリオン病4例の計31例の症例に対し，300 mg/dayを経口，あるいは経管投与にて12週間の連続投与というプロトコールで臨床研究が行われた．その結果，12例で覚醒度や自発語，注視など，臨床症状に一過的な改善が認められたが(効果が認められた例：孤発性9例，医原性2例，遺伝性1例)，その後，効果は消失した．16例に肝機能障害や溶血性貧血などの重大な副作用が認められ，より毒性の低い塩酸キニーネに変更されたが，持続的な薬効を保つことと副作用を抑えることが困難であった[21]．

PPSについては，英国を中心に13例の治療が行われてきた．わが国では福岡大学にて臨床試験が行われている[22]．PPSはBBBを透過しないため，微量注入器具を用いて脳室内へ連続投与することが検討され，動物実験では脳内接種後10日からの投与で173％，30日からの投与で93％の潜伏期の延長が認められた[15]．本薬剤は，2003年，英国において1例の変異型CJD患者にて臨床研究が開始されたが，脳の萎縮の進行は止まらなかったものの副作用は認められず，臨床症状は落ち着いており，現在まだ経過を観察中である．わが国でも，さまざまなプリオン病患者で臨床研究が開始されており，その効果と副作用について解析が進められている[23]．PPSを用いた脳室内持続投与療法は，英国や日本以外の国でも開始され，全世界で20例近い患者に実施されており，現在最も期待されている治療法のひとつといえる．今後，最適の治療プロトコールの完成と，臨床症状の改善が判断できる症例での検討が求められる．

フルピルチンは，非オピオイド系の中枢性鎮痛薬として臨床で用いられてきたが，細胞培養実験などから神経細胞死を抑制する効果が再発見されて以来，神経変性疾患への治療に応用されるようになってきた．CJD患者については，28名の患者において二重盲検試験として臨床試験が行われた[24]．その結果，フルピルチンはCJDの認知機能の低下を有意に抑制したものの，CJDの進行を抑制することはできなかった．

おわりに

プリオン病は通常の細菌やウイルスなどを介した感染症と異なり，感染してからの潜伏期が長く，発症直前まで感染の有無を知ることができない．加えて，急速に進む神経変性を治療していくことは非常に難解な問題となっている．末梢から中枢神経への感染を予防することは，現在開発されているいくつかの薬剤でも可能と思われるが，それには発症前に治療を開始することが必須であり，現在のところ，医原性プリオン病や遺伝性プリオン病など，将来発症する可能性のある人には応用することができるものの，実際的ではない．MRI拡散強調画像や脳脊髄液中の14-3-3蛋白質などが神経変性初期の診断の助けになることが報告されているが，より早い時期での診断のためのマーカーの検索や検出法の開発が求められている．血液や尿中のPrP^{Sc}の高感度検出は，感染初期あるいは発症初期の検出法となるかもしれない．従来，PrP^{Sc}が神経変性の原因と考えられていたが，いくつかの実験から，PrP^{C}あるいはPrP^{C}からPrP^{Sc}に変化する中間体が神経変性を引き起こすとの仮説が提唱されている．必ずしもPrP^{Sc}の増殖を防げなくとも，神経変性のメカニズムを明らかにし，神経変性の進行を抑制する薬剤の探索や治療法を開発することは，プリオン病の治療法のひとつのゴールでもある．こちらの展開にも期待したい．

●文 献
1) Prusiner SB : Proc Natl Acad Sci USA 95 : 13363-13383, 1998
2) Race RE, Fadness LH, Chesebro B : J Gen Virol 68 : 1391-1399, 1987
3) Klohn PC, Stoltze L, Flechsig E et al : Proc Natl Acad Sci USA 100 : 11666-11671, 2003
4) Prusiner SB, Cochran SP, Groth DF et al : Ann Neurol 11 : 353-358, 1982
5) Kitamoto T, Mohri S, Ironside JW et al : Biochem Biophys Res Commun 294 : 280-286, 2002
6) Bach S, Talareki N, Andrieu T et al : Nat Biotechnol 21 : 1075-1081, 2003
7) Bertsch U, Winklhofer KF, Hirschberger T et al : J Virol 79 : 7785-7791, 2005
8) Kawatake S, Nishimura Y, Sakaguchi S et al : Biol Pharm Bull 29 : 927-932, 2006
9) Bellon A, Seyfert-Brandt W, Lang W et al : J Gen Virol 84 : 1921-1925, 2003
10) Castilla J, Saa P, Soto C : Nat Med 11 : 982-985, 2005
11) Trevitt CR, Collinge J : Brain 129 : 2241-2265, 2006
12) Caughey B, Race RE : J Neurochem 59 : 768-771, 1992
13) Tagliavini F, McArthur RA, Canciani B et al : Science 276 : 1119-1122, 1997
14) Forloni G, Iussich S, Awan T : Proc Natl Acad Sci USA 99 : 10849-10854, 2002
15) Amyx H, Salazar AM, Gajdusek CD et al : Neurol 34 (Suppl 1), 1984
16) Doh-ura K, Ishikawa K, Murakami-Kubo I et al : J Virol 78 : 4999-5006, 2004
17) Soto C, Kascsack RJ, Saborio GP et al : Lancet 355 : 192-197, 2000
18) Kocisko DA, Caughey WS, Race RE et al : Antimicrob Agents Chemother 50 : 759-761, 2006
19) Doh-Ura K, Iwaki T, Caughey B : J Virol 74 : 4894-4897, 2000
20) Korth C, May BC, Cohen FE, Prusiner SB : Proc Natl Acad Sci USA 98 : 9836-9841, 2001
21) Muller WE, Ushijima H, Schroder HC et al : Eur J Pharmacol 246 : 261-267, 1993
22) 山田達夫, 坪井義夫, 中島雅士ほか：厚生労働省科学研究費補助金こころの健康科学研究事業, 即戦力的クロイツフェルト・ヤコブ病治療法の確立に関する研究(主任研究者 堂浦克美), 平成15年度総括研究報告書, pp11-22
23) Rainov NG, Whittle IR, Doh-ura K : Prions－Food and Drug Saftey. (Kitamoto T ed) Springer-Verlag, Tokyo, 2005
24) Otto M, Cepek L, Ushijima H et al : Neurol 62 : 714-718, 2004

Human Molecular Genetics, 2006, Vol. 15, No. 10 **1600–1609**
doi:10.1093/hmg/ddl081
Advance Access published on March 29, 2006

WFS1-deficiency increases endoplasmic reticulum stress, impairs cell cycle progression and triggers the apoptotic pathway specifically in pancreatic β-cells

Takahiro Yamada[1], Hisamitsu Ishihara[1,*], Akira Tamura[1], Rui Takahashi[1], Suguru Yamaguchi[1], Daisuke Takei[1], Ai Tokita[1], Chihiro Satake[1], Fumi Tashiro[3], Hideki Katagiri[2], Hiroyuki Aburatani[4], Jun-ichi Miyazaki[3] and Yoshitomo Oka[1]

[1]Division of Molecular Metabolism and Diabetes and [2]Division of Advanced Therapeutics for Metabolic Diseases, Tohoku University Graduate School of Medicine, 2-1 Seiryo-machi, Aoba-ku, Sendai, Miyagi 980-8575, Japan, [3]Division of Stem Cell Regulation Research, Osaka University Graduate School of Medicine, Suita, Osaka 565-0871, Japan and [4]Genome Science Division, Research Center for Advanced Science and Technology, The University of Tokyo, Tokyo 153-8904, Japan

Received January 28, 2006; Revised and Accepted March 24, 2006

Wolfram syndrome, an autosomal recessive disorder associated with diabetes mellitus and optic atrophy, is caused by mutations in the *WFS1* gene encoding an endoplasmic reticulum (ER) membrane protein. Herein, we report that pancreatic islets of *wfs1*-deficient mice exhibit increases in phosphorylation of RNA-dependent protein kinase-like ER kinase, chaperone gene expressions and active XBP1 protein levels, indicating an enhanced ER stress response. We established *wfs1*-deficient MIN6 clonal β-cells by crossing *wfs1*-deficient mice with mice expressing simian virus 40 large T antigen in β-cells. These cells show essentially the same alterations in ER stress responses as *wfs1*-deficient islets, which were reversed by re-expression of WFS1 protein or overexpression of GRP78, a master regulator of the ER stress response. In contrast, these changes are not observed in heart, skeletal muscle or brown adipose tissues with WFS1-deficiency. The increased ER stress response was accompanied by reduced BrdU incorporation and increased caspase-3 cleavage, indicating impaired cell cycle progression and accelerated apoptotic processes in the mutant islets. These changes are associated with increased expression of the cell cycle regulator $p21^{CIP1}$ in *wfs1*-deficient islets and clonal β-cells. Treatment of islets with thapsigargin, an ER stress inducer, caused upregulation of $p21^{CIP1}$. In addition, forced expression of $p21^{CIP1}$ resulted in reduced MIN6 β-cell numbers, suggesting the ER stress-induced increase in $p21^{CIP1}$ expression to be involved in β-cell loss in the mutant islets. These data indicate that WFS1-deficiency activates the ER stress response specifically in β-cells, causing β-cell loss through impaired cell cycle progression and increased apoptosis.

INTRODUCTION

Type 2 diabetes is caused by complex interactions between insulin resistance in peripheral tissues and impaired insulin secretion from pancreatic β-cells. There is a general consensus that the latter results from both impaired β-cell function and decreased β-cell mass (1–3). Adult β-cell mass is maintained by a balance between generation and death of β-cells. In patients with type 2 diabetes, new islet formation and β-cell replication are reportedly normal, and an increased rate of apoptosis has been suggested to underlie the loss of β-cell mass (4).

Recent studies using novel mutant mice have led to new insights into endoplasmic reticulum (ER) stress and maintenance

*To whom correspondence should be addressed. Tel: +81 227177611; Fax: +81 227177612; Email: hisamitsu-ishihara@mail.tains.tohoku.ac.jp

of β-cell mass (5,6). The ER stress response, also known as the unfolded protein response (UPR), involves translational attenuation, transcriptional induction of chaperones and folding enzymes, as well as degradation of misfolded proteins, a process called ER-associated degradation (ERAD). When ER stress is strong and cellular survival mechanisms fail to correct the protein-folding defects, an ER stress-mediated apoptotic process is initiated (5–7). Mice with a homozygous null mutation of RNA-dependent protein kinase-like ER kinase (PERK) lose their ability to phosphorylate eukaryotic initiation factor 2α (eIF2α) and fail to attenuate translation in response to ER stress. These mice develop diabetes owing to reduced β-cell mass (8). Importantly, mutations of the *EIF2AK3* gene encoding PERK in humans have been recognized as causing Wolcott-Rallison syndrome with diabetes mellitus in early infancy (9). A mouse model in which a Ser51Ala mutation of eIF2α prevents the protein from being phosphorylated by PERK and other eIF2α kinases, also displays a β-cell defect and impaired gluconeogenesis leading to lethal hypoglycemia (10). Mice with a deletion mutation of $P58^{IPK}$, a cytosolic chaperone, were recently reported to exhibit β-cell failure and diabetes (11). These examples suggest that β-cells, producing large quantities of insulin and thus a greater load on the ER, are especially sensitive to ER stress.

Wolfram syndrome is a rare autosomal recessive disorder characterized by juvenile-onset diabetes mellitus, optic atrophy, diabetes insipidus and sensorineural deafness (12). This syndrome is caused by mutations in the *WFS1* gene (13,14), which encodes an ER resident membrane protein (15). Post-mortem studies of the pancreas from subjects with Wolfram syndrome have shown β-cell loss (16). We recently established a line of mutant mice with a disrupted *wfs1* gene and found that these mice also exhibited impaired glucose homeostasis accompanied by a progressive reduction of β-cell mass (17). Thus, the *wfs1*-deficient mouse is a model for studying mechanisms of β-cell loss during the development of diabetes in Wolfram syndrome. We and others have also shown expression of WFS1 protein to be up-regulated by ER stress-inducing agents (18–20). A recent study employing IRE1α knockout and PERK knockout cells suggested that WFS1 is a component of the IRE1 and PERK signaling pathways (20). In addition, *wfs1*-deficient islets have been shown to exhibit increased DNA fragmentation in response to ER stress inducers (17), suggesting β-cell loss in Wolfram syndrome to be attributable to an inability to handle ER stress. A very recent study of islets conditionally lacking the *wfs1* gene in β-cells, demonstrated an increased GRP78 mRNA to GLUT2 mRNA ratio. This observation was interpreted as evidence of an enhanced ER stress response, on the assumption that GLUT2 mRNA levels represented the β-cell number in islets (21).

To further investigate the mechanisms underlying β-cell loss in Wolfram syndrome, we conducted a systematic study of the UPR in *wfs1*-deficient islets as well as other tissues. We also created β-cell lines with WFS1-deficiency and studied UPR. We found all three UPR subpathways to be activated in *wfs1*-deficient islets and β-cell lines. Furthermore, we demonstrated increased cleavage of caspase-3, a hallmark of apoptosis, and impaired proliferation associated with enhanced expression of the cell cycle regulator $p21^{CIP1}$.

RESULTS

UPR activation in *wfs1*-deficient islets

A systematic study of the UPR was conducted using islets isolated from 6-week-old male *wfs1*-deficient mice with the C57Bl/6 background. At 6 weeks of age, the β-cell mass of these mice begins to decrease (17). Accumulation of unfolded proteins in the ER is well known to induce dissociation of GRP78 from PERK, resulting in oligomerization and subsequent auto-phosphorylation of PERK. Activated PERK then phosphorylates eIF2α and suppresses general protein translation to reduce the ER load (5–7). In freshly isolated *wfs1*-deficient islets, PERK phosphorylation was increased (Fig. 1A). In addition, eIF2α phosphorylation was slightly but significantly enhanced with no alteration in total eIF2α levels in mutant islets (Fig. 1A). Thus, the ratio of phosphorylated eIF2α over total eIF2α levels analyzed by densitometry was increased by $27 \pm 7\%$ ($n = 4$ experiments, $P < 0.05$). These data indicate that one of three subpathways of the UPR arising from PERK phosphorylation is initiated in response to WFS1-deficiency in islets.

ER stress is also sensed by other ER resident proteins, IRE1 and ATF6, in addition to PERK (5–7). Activation of ATF6 via GRP78 dissociation and subsequent cleavage is known to induce the expressions of various chaperone genes, constituting another subpathway of the UPR (5–7). In *wfs1*-deficient islets, GRP94 mRNA levels were increased and those of GRP78 and $P58^{IPK}$ also tended to rise (Fig. 1B). Correspondingly, although the differences failed to reach statistical significance, levels of these chaperone proteins tended to be increased (Fig. 1C), suggesting that the ATF6 subpathway of the UPR is activated in response to WFS1-deficiency.

As shown in Figure 1D, a shorter form of XBP1 mRNA was increased. This form is produced by 26-nucleotide splicing from primary XBP1 mRNA by the ribonuclease activity of IRE1, increasing active XBP1 protein levels in mutant islets (Fig. 1E). HRD1, a ubiquitin ligase involved in ERAD, is one of the XBP1 target genes (22). In *wfs1*-deficient islets, levels of HRD1 protein were markedly increased (Fig. 1E). In addition, mRNA levels of ER-associated degradation-enhancing α-mannosidase-like protein (EDEM) (23), another target of XBP1, were significantly increased in mutant islets [100 ± 5 arbitrary units (wild-type) versus 136 ± 18 (mutant), $n = 6$, $P < 0.05$]. These data indicate that the IRE1-initiated subpathway of the UPR is also activated in *wfs1*-deficient islets.

Establishment of MIN6 β-cell lines deficient in WFS1

To examine the influence of WFS1-deficiency specifically in a homogenous β-cell population, β-cell lines were established by crossing $wfs1^{+/-}$ and $wfs1^{-/-}$ mice (17) with IT6 mice expressing simian virus 40 (SV40) large T antigen under the insulin promoter (24) and were designated MIN6wfs1$^{+/-}$ and MIN6wfs1$^{-/-}$, respectively (see Materials and Methods). IT6 mice were previously reported to develop insulinoma, from which the MIN6 cell line (24), one of the most highly differentiated β-cell lines, was generated. We established two cell lines each for the $wfs1^{+/-}$ and $wfs1^{-/-}$ genotypes. As shown in Figure 2A, the two cell lines with the $wfs1^{-/-}$ genotype (MIN6wfs1$^{-/-}$ – 1 and 2) show similar UPR

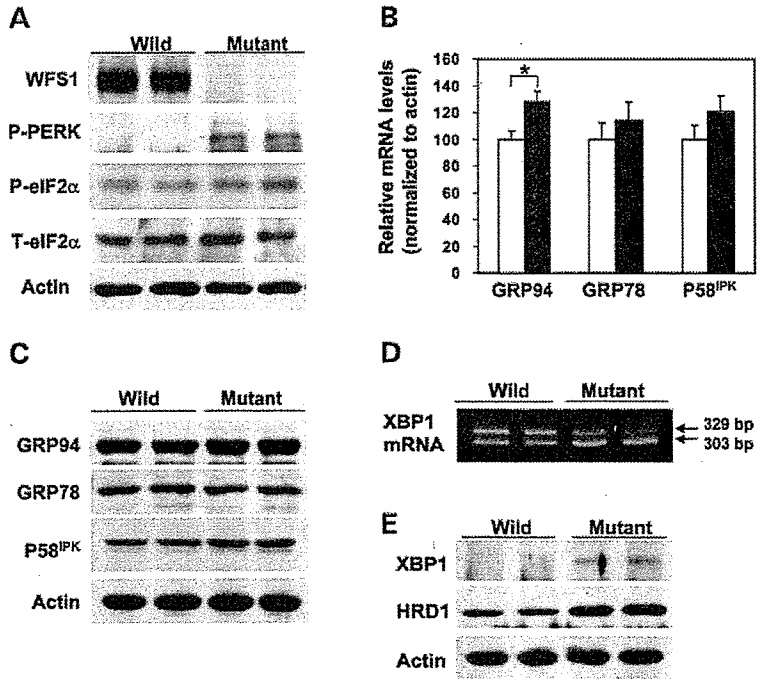

Figure 1. Activation of three subpathways of the UPR in *wfs1*-deficient islets. (**A**) Activation of the PERK/eIF2α pathway. Islets isolated from wild-type and *wfs1*-deficient mice were subjected to SDS–PAGE and probed with the indicated antibodies: P-PERK, phosphorylated-PERK; P-eIF2α, phosphorylated-eIF2α; T-eIF2α, total eIF2α. (**B**) Real-time RT–PCR analysis of GRP94, GRP78 and $P58^{IPK}$ gene expressions in wild-type (open columns) and *wfs1*-deficient (closed columns) mice. Relative mRNA levels were obtained after normalization to actin mRNA. $^*P < 0.05$, $n = 6$. (**C**) Expressions of chaperone proteins in *wfs1*-deficient islets. Lysates of isolated islets were probed with the indicated antibodies. (**D**) Increased XBP1 mRNA splicing in *wfs1*-deficient islets. Amplification of XBP1 mRNA from islet total RNA with specific primers yields spliced (303 bp) and non-spliced (329 bp) XBP1 transcripts. (**E**) Activation of the IRE1/XBP1 pathway. Lysates of isolated islets were probed with the indicated antibodies. Western blot data shown are representative of at least three experiments with different sets of samples.

characteristics. Similarly, characteristics of two cell lines with the *wfs1*$^{+/-}$ genotype (MIN6wfs1$^{+/-}$) were indistinguishable (data not shown). Therefore, only one line of each genotype was used for subsequent analyses. We compared MIN6wfs1$^{-/-}$ with MIN6wfs1$^{+/-}$ at the same passage numbers (passages 5–8), but not with the original MIN6 cells. This is because we were concerned that a difference in passage number between the original MIN6 and MIN6wfs1$^{-/-}$ cells, irrespective of WFS1-deficiency, might affect the protein expression profile, rendering the former an inappropriate control for the latter. After completion of a series of experiments, MIN6wfs1$^{+/-}$ cells reached passages 15–20, the same passage of original MIN6 cells we have. The function and survival of MIN6wfs1$^{+/-}$ cells are similar to those of wild-type MIN6 cells at similar passage numbers (data not shown).

Effects of WFS1-deficiency on UPR in β-cell lines

As shown in Figure 2A, altered expressions of UPR-related proteins observed in *wfs1*-deficient islets were reproduced in MIN6wfs1$^{-/-}$ cells; PERK phosphorylation, as well as expressions of active XBP1 and HRD1, were increased in *wfs1*-deficient MIN6 cells. ATF4 levels were also shown to be increased in these cells. Furthermore, although GRP78 and GRP94 protein levels were similar (Fig. 2B, upper panel), the activity of the GRP78 promoter containing three ER stress response elements was greater in MIN6wfs1$^{-/-}$ cells than in MIN6wfs1$^{+/-}$ cells (Fig. 2B), strongly suggesting activation of the ATF6 subpathway of the UPR in MIN6wfs1$^{-/-}$ cells. To confirm that alterations in UPR-related proteins are due to WFS1-deficiency, wild-type human WFS1 protein was expressed in MIN6wfs1$^{-/-}$ cells. We took advantage of the tetracycline-inducible expression system. MIN6wfs1$^{-/-}$ cells were infected with the Tet-repressor expressing virus (AdCAG-TR) together with a recombinant adenovirus bearing wild-type human WFS1 cDNA under the CMV promoter containing the Tet-operator (AdCTO-WFS1). The cells were then treated with doxycycline (2 μg/ml). As shown in Figure 2C, when WFS1 expression was restored to levels comparable to those of the original MIN6 cells, the increase in PERK phosphorylation was prevented. In addition, overexpression of GRP78, a master regulator of the ER stress response, also resulted in normalization of PERK phosphorylation levels (Fig. 2D), clearly indicating the observed alteration in UPR-related proteins to be due to exacerbation of ER stress caused by WFS1-deficiency.

No UPR induction in heart, skeletal muscle or brown adipose tissues from *wfs1*-deficient mice

WFS1 protein is expressed in a variety of non-pancreatic tissues, though less abundantly than in islets (Fig. 3A).

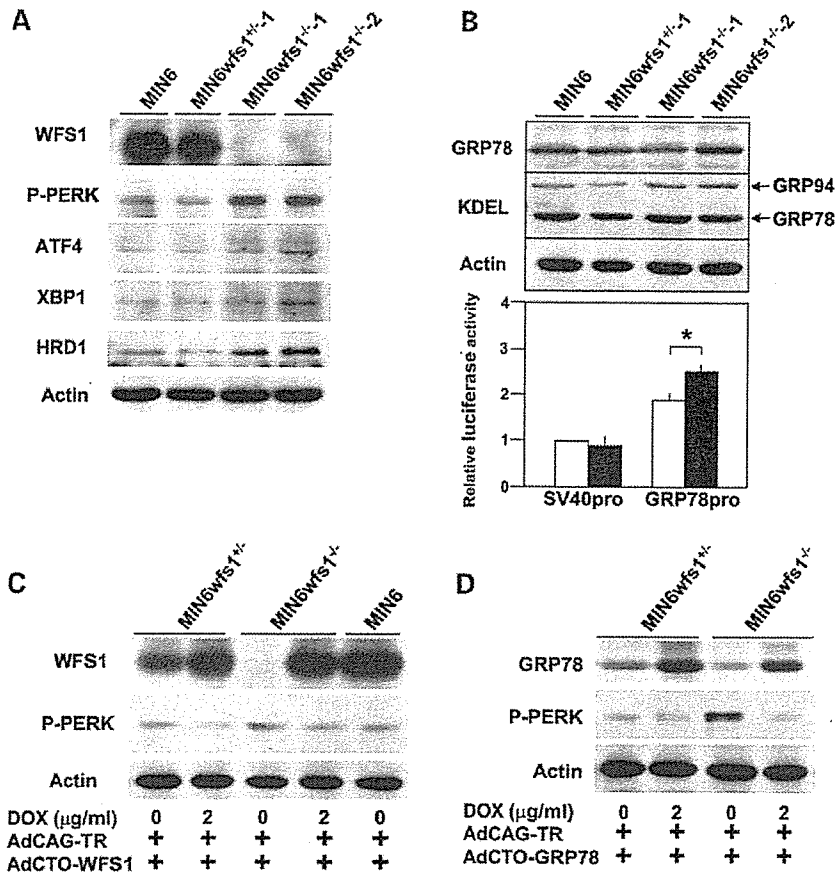

Figure 2. Increased UPR and its reversal by expression of WFS1 or GRP78 in an SV40 transformed *wfs1*-deficient β-cell line (MIN6wfs1$^{-/-}$). (**A**) Expression of UPR-related proteins in various MIN6 cell lines. MIN6, MIN6wfs1$^{+/-}$ − 1, MIN6wfs1$^{-/-}$ − 1 and MIN6wfs1$^{-/-}$ − 2 cells were lysed and probed with the indicated antibodies. Data shown are representative of at least three experiments with different sets of samples. (**B**) Expressions of chaperone proteins in MIN6wfs1$^{-/-}$ cells. (Upper panel) Cellular lysates were probed with anti-GRP78, anti-KDEL and anti-actin (loading control) antibodies. (Lower panel) MIN6wfs1$^{+/-}$ (open columns) and MIN6wfs1$^{-/-}$ (closed columns) cells were transiently transfected with the pGL3-promoter plasmid containing the SV40 promoter-luciferase (SV40pro: 0.5 μg) or pGRP78pro(−172)-Luc (GRP78pro: 0.5 μg) together with the reference plasmid pTK-RL (0.05 μg) encoding *Renilla* luciferase. Twenty-four hours after transfection, cellular lysates were subjected to luciferase assay. The luciferase activity of the pGL3-promoter in MIN6wfs1$^{+/-}$ was defined as 1. The averages of three independent experiments, each performed in duplicate, are presented. *$P < 0.05$, $n = 3$. (**C**) Suppression of PERK phosphorylation by WFS1 re-expression in MIN6wfs1$^{-/-}$ cells. Cells were infected with AdCAG-TR expressing Tet-repressor and AdCTO-WFS1 harboring *WFS1* cDNA. WFS1 expression was induced by 48 h doxycycline (DOX, 2 μg/ml) treatment. The experiment was repeated three times and similar results were obtained. (**D**) Suppression of PERK phosphorylation by GRP78 overexpression in MIN6wfs1$^{-/-}$ cells. Human GRP78 expression was induced by 48 h DOX treatment. The experiment was repeated four times and similar results were obtained.

Therefore, we also examined expressions of UPR genes in tissues other than pancreatic islets. Cardiac function is reportedly not impaired in subjects with Wolfram syndrome (12) or in *wfs1*-deficient mice (17). Skeletal muscle and brown adipose tissue also appear essentially normal in mutant mice (data not shown). In contrast to islets, no UPR alterations were observed in these tissues from *wfs1*-deficient mice (Fig. 3B–D). Thus, UPR activation is tissue-specific in WFS1-deficiency.

Increased β-cell apoptotic response in *wfs1*-deficient islets

ER stress induces apoptosis through activation of various signaling molecules including JNK and pro-apoptotic proteins, such as CHOP (5–7). CHOP expression was increased at both the mRNA (Fig. 4A) and the protein level (Fig. 4B), in mutant when compared with wild-type islets. In contrast, JNK expression levels and phosphorylation states were not altered in *wfs1*-deficient islets (Fig. 4B). We also found increased levels of cleaved caspase-3, a hallmark of apoptosis, in mutant islets (Fig. 4B). CHOP expression and cleaved caspase-3 levels were also increased in *wfs1*-deficient MIN6 cells (Fig. 4C), whereas no such changes were observed in heart, skeletal muscle or adipose tissue (data not shown).

We also measured apoptosis in MIN6wfs1$^{-/-}$ and MIN6wfs1$^{+/-}$ cells by counting adherent cells positive for annexin V staining under fluorescent microscope. We found 1–2% cells to be annexin V positive for both the *wfs1*$^{-/-}$ and the *wfs1*$^{+/-}$ genotype cultured under standard conditions, i.e. no differences between MIN6wfs1$^{-/-}$ and MIN6wfs1$^{+/-}$

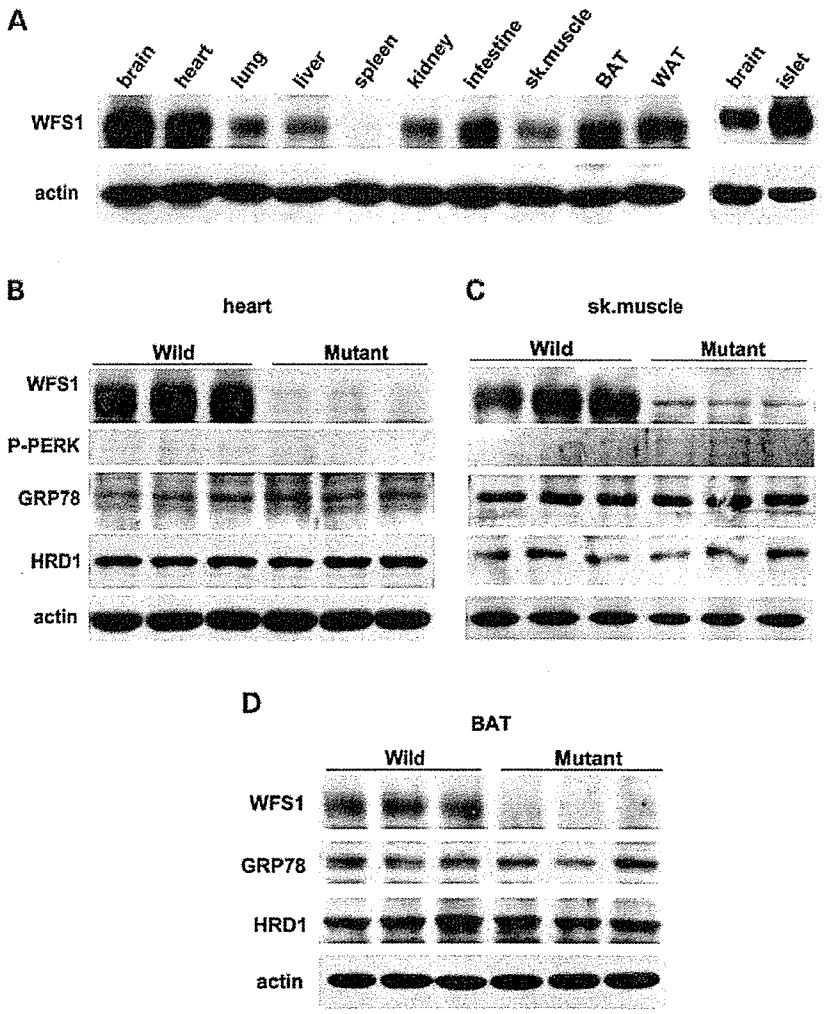

Figure 3. No UPR changes in heart, skeletal muscle or brown adipose tissue from *wfs1*-deficient mice. (**A**) WFS1 protein distribution in mice. Approximately, 100 μg of protein from wild-type mouse tissues were analyzed for the presence of WFS1 protein. BAT, brown adipose tissue; WAT, white adipose tissue. (**B–D**) UPR activation was not observed in heart (B), skeletal muscle (C) or BAT (D) from *wfs1*-deficient mice. The western blot data shown are representative of two experiments, each performed using three mice of each genotype.

cells. An increase in the number of apoptotic cells was observed when MIN6wfs1$^{-/-}$ cells were challenged with 0.5 μM thapsigargin (TG) for 24 h, as compared with MIN6wfs1$^{+/-}$ cells under the same conditions [2.7 ± 1.0% (MIN6wfs1$^{+/-}$) versus 6.2 ± 1.1% (MIN6wfs1$^{-/-}$) $n = 3$, $P < 0.05$]. Therefore, MIN6wfs1$^{-/-}$ cells exhibited increased apoptosis susceptibility. These data, together, indicate that an ER stress mediated-apoptotic process is activated in *wfs1*-deficient β-cells.

Impaired β-cell proliferation in *wfs1*-deficient islets

In addition to increased apoptosis, decreased proliferation may contribute to loss of β-cell mass in *wfs1*-deficient mice. When β-cell proliferation activity was assayed by 5-bromodeoxyuridine (BrdU) incorporation in pancreases from wild-type and mutant mice, BrdU incorporation was found to be significantly reduced in *wfs1*-deficient β-cells (Fig. 5A and B). This observation suggested impaired proliferation, along with increased apoptosis, to contribute to β-cell loss in *wfs1*-deficient islets.

We next explored possible causes of the decreased β-cell proliferation in *wfs1*-deficient islets. The link between the UPR and cell cycle arrest was previously reported to be mediated by down-regulation of cyclin D1 because of general translational suppression via eIF2α phosphorylation (25). However, neither expression of cyclin D1 nor that of cyclin D2, major isoforms of the D type cyclins in β-cells (26,27), was changed in mutant islets (data not shown). CHOP has also been recognized as causing cell cycle arrest and apoptosis (28,29). As GADD34 is reportedly a target of CHOP (30) and is involved in cell growth and survival (31),

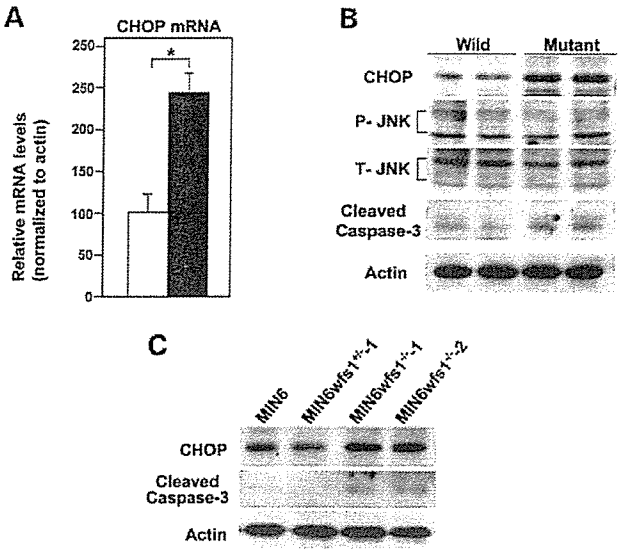

Figure 4. Activation of apoptosis signaling in *wfs1*-deficient islets and MIN6 cells. (A) Real-time RT–PCR analysis of CHOP mRNA in wild-type (open column) and *wfs1*-deficient (closed column) islets. Relative mRNA levels were obtained after normalization to actin mRNA. $^{*}P < 0.05$, $n = 6$. (**B**) Western blot analysis of apoptosis signaling proteins in *wfs1*-deficient islets. Lysates of islets were probed with the indicated antibodies: P-JNK, phospho-JNK; T-JNK, total-JNK. Data shown are representative of three experiments with different sets of samples. (**C**) Increased expression of CHOP and cleaved caspase-3 in *wfs1*-deficient MIN6 cells. Lysates of MIN6 cell derivatives were probed with the indicated antibodies. Data shown are representative of three experiments.

GADD34 expression was examined. GADD34 transcript levels were found to be increased in *wfs1*-deficient islets (100 ± 11 versus 151 ± 14, $P < 0.05$). Recent studies have demonstrated that cell cycle regulation is critical for maintenance of β-cell mass (25,26). As GADD34 reportedly induces p53 phosphorylation and enhances expression of the cell cycle inhibitor $p21^{CIP1}$ (32), p53 and $p21^{CIP1}$ expressions were assessed. We found phosphorylation of p53 to be increased, though total p53 was not elevated (Fig. 5C). In addition, increased expressions of $p21^{CIP1}$ mRNA (100 ± 11 versus 413 ± 32, $P < 0.01$) and $p21^{CIP1}$ protein (Fig. 5C) were observed in *wfs1*-deficient islets. We also examined the expression of another cell cycle inhibitor, $p27^{KIP1}$, and found no difference between wild-type and mutant islets (Fig. 5C). Increased expression of $p21^{CIP1}$ protein was also observed in *wfs1*-deficient MIN6 cells, SV40 large T antigen-transformed cells in which p53 activity was considered to be suppressed (Fig. 5D). Expression of $p21^{CIP1}$ protein was not increased in heart, skeletal muscle or brown adipose tissues from *wfs1*-deficient mice (data not shown).

In order to determine whether increased expression of $p21^{CIP1}$ is attributable to ER stress, wild-type islets were treated with TG (0.5 μM) for 12 h. As shown in Figure 5E, expression of $p21^{CIP1}$ was significantly increased. In addition, expression of $p21^{CIP1}$ was markedly increased in MIN6 cells treated with TG (Fig. 5F) or tunicamycin (data not shown). These data suggest 21^{CIP1} expression to be induced by ER stress in β-cells.

Finally to assess the effects of $p21^{CIP1}$ expression on β-cell proliferation, $p21^{CIP1}$ was expressed in wild-type MIN6 cells in a tetracycline-inducible manner (Fig. 6A). Overexpression of $p21^{CIP1}$ suppressed a MIN6 cell number increase (Fig. 6B), suggesting that increased $p21^{CIP1}$ expression contributes to the reduced β-cell mass in *wfs1*-deficient islets.

DISCUSSION

We systematically investigated UPR in *wfs1*-deficient islets and MIN6 β-cells as well as heart, skeletal muscle and brown adipose tissues from the mutant mice in this study. Enhanced UPR was specifically observed in β-cells but not in other tissues examined. These findings indicate that diabetes in Wolfram syndrome is caused by increased ER stress in β-cells and establish Wolfram syndrome as an ER stress-based disease, as is the case in Wolcott-Rallison syndrome with PERK-deficiency (9). Furthermore, we found enhanced UPR to be associated with not only activation of the apoptotic pathway but also impaired cell cycle progression in β-cells. These observations provide evidence of novel mechanisms underlying ER stress-mediated β-cell loss.

We demonstrated activation of the PERK and IRE1 subpathways of the UPR. Increased activation of the GRP78 promoter indicates the ATF6 subpathway to be induced as well. GRP78 expression was also reportedly increased by knockdown of WFS1 expression in INS1 insulinoma β-cells (20). Collectively, these data indicate that all three UPR subpathways are activated by WFS1-deficiency in β-cells. The UPR is activated when ER homeostasis is perturbed by defective ER calcium homeostasis, mutations in ER resident proteins and/or abnormalities of the ERAD system. Disturbed ER homeostasis is also induced by defect(s) in components of the UPR system, as is the case in Wolcott-Rallison syndrome with PERK-deficiency. The present data suggest that impaired ER homeostasis does not result from defect(s) in a specific pathway(s) of the UPR. Our previous study demonstrated an abnormal cytosolic Ca^{2+} response in *wfs1*-deficient β-cells (17), suggesting that impaired ER Ca^{2+} homeostasis is a possible cause of ER stress associated with WFS1-deficiency.

We found that WFS1 protein is highly expressed in heart, skeletal muscle and brown adipose tissues. However, there is no UPR activation in these tissues from mutant mice. Thus, the UPR is tissue-specific in *wfs1*-deficient mice. One possible explanation of this tissue specificity is that a protein(s), compensating for loss of WFS1 protein function is present in these tissues but not in β-cells. This interesting possibility merits further investigation and elucidation of WFS1 function is necessary to resolve the tissue-specific effects of WFS1-deficiency.

Our results demonstrate, in addition to the augmented apoptotic process evidenced by increased caspase-3 cleavage, that β-cell proliferation is decreased in *wfs1*-deficient mice. Impaired proliferation was also reported in BRIN-BD11 cells expressing the human WFS1 antisense transcript (33). Our observation is in contrast to that by Riggs *et al.* (21) who detected no changes in the numbers of BrdU-positive cells in islets from β-cell specific *wfs1* knockout mice. The reason for this discrepancy is currently unclear, but may

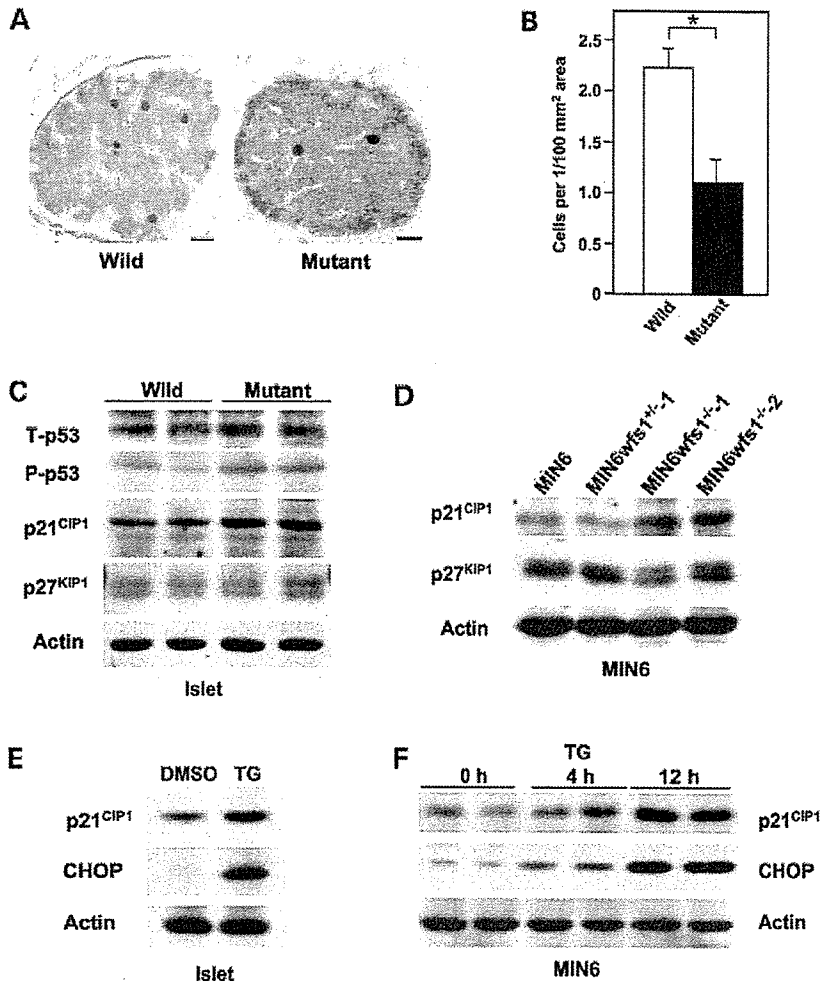

Figure 5. Impaired cell cycle progression and increased $p21^{CIP1}$ expression in *wfs1*-deficient islets. (**A** and **B**) Impaired cell cycle progression in *wfs1*-deficient β-cells. Incorporated BrdU and insulin were probed with specific antibodies (A) and BrdU positive β-cells were counted (B). Bars, 10 μM. $^*P < 0.05$, $n = 4$ mice per group. (**C** and **D**) Increased $p21^{CIP1}$ expression in *wfs1*-deficient islets and MIN6 cells. Lysates of wild-type and *wfs1*-deficient islets (C) or MIN6 cells (D) were probed with the indicated antibodies: T-p53, total-p53; P-p53, phospho-p53. Data shown are representative of three experiments with different sets of samples. (**E** and **F**) Induction of $p21^{CIP1}$ expression by TG in islets (E) and MIN6 cells (F). Wild-type islets were challenged with 0.5 μM TG for 12 h. MIN6 cells were also treated with 0.5 μM TG for the indicated durations. Lysates of islets or MIN6 cells were probed with the indicated antibodies. The experiment was repeated three times and similar results were obtained.

reflect differences in the ages of the mice studied: 6-week-old mice were used in the present versus 12- or 24-week-old animals in their study (21). Cell cycle dysregulation in *wfs1*-deficient islets was associated with increased expression of $p21^{CIP1}$, a cell cycle regulator. $p21^{CIP1}$ can serve, depending on which tissues or cells it is activated in, as both an inhibitor and an agonist of cell cycle progression (34). Our observation that forced expression of $p21^{CIP1}$ suppressed MIN6 β-cell proliferation suggests that $p21^{CIP1}$ operates as a cell cycle inhibitor in β-cells, although our results must be interpreted cautiously, as forced overexpression of $p21^{CIP1}$ may produce effects different from those occurring in mutant β-cells with increased $p21^{CIP1}$ levels. A very recent study, demonstrating that $p21^{CIP1}$ acts as a molecular brake on mitogenic stimuli in β-cells (35), supports the notion of $p21^{CIP1}$ functioning as a cell cycle inhibitor in β-cells. ER stress inducers were recently reported to cause $p21^{CIP1}$ expression and cell cycle arrest in chondrocytes (36) and prostatic cancer cells (37), suggesting that cell cycle arrest associated with increased $p21^{CIP1}$ expression is a common feature in cells under ER stress. Furthermore, reduced proliferation associated with increased expression of $p21^{CIP1}$, in *wfs1*-deficient β-cells (the present study) and β-cells transgenic for hepatocyte growth factor and/or placental lactogen (35), highlights an important role for $p21^{CIP1}$ in regulation of β-cell mass in addition to the roles of $p27^{KIP1}$ recently reported (38).

CHOP induces GADD34 expression (30), which then activates p53 phosphorylation and $p21^{CIP1}$ transcription (32). Therefore, the CHOP → GADD34 → p53 pathway is a candidate for ER stress-mediated $p21^{CIP1}$ expression. Indeed,

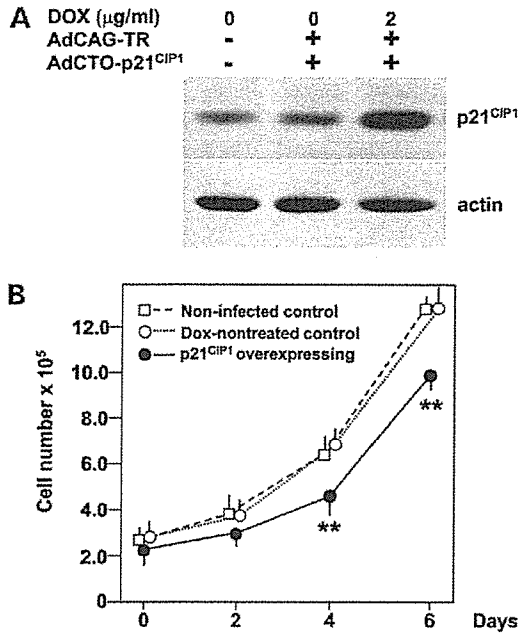

Figure 6. Decrease in MIN6 cell numbers in response to forced $p21^{CIP1}$ expression. (**A**) Forced expression of $p21^{CIP1}$ in MIN6 cells. Cells were either uninfected or infected with AdCAG-TR (m.o.i. of 30) and AdCTO-$p21^{CIP1}$ (m.o.i. of 100) harboring $p21^{CIP1}$ cDNA. Expression of $p21^{CIP1}$ was induced by 48 h DOX (2 μg/ml) treatment. MIN6 cell lysates were subjected to immunoblot analysis using anti-$p21^{CIP1}$ and actin antibodies. (**B**) Numbers of MIN6 cells overexpressing $p21^{CIP1}$. One day after adenovirus transduction, cells were reseeded (2×10^5 per well) and divided into two groups, and, after two more days, treatment with (closed circles) or without (open circles) DOX (2 μg/ml) was commenced (day 0). Uninfected MIN6 cells (open squares) were also seeded 2 days before. Cells were then harvested on days 0, 2, 4 and 6, stained with trypan blue and counted. Data are means ± S.E. for triplicate wells. $^{**}P < 0.01$ against both controls. The experiment was repeated three times and similar results were obtained.

an increase in $p21^{CIP1}$ expression was associated with increased GADD34 expression and p53 phosphorylation in *wfs1*-deficient β-cells. However, induction of $p21^{CIP1}$ expression by TG was observed in MIN6 cells transformed with SV40 large T antigen, a well-known suppressor of p53. In addition, an ER stress-induced increase in $p21^{CIP1}$ expression was observed in p53-deficient prostatic cancer cells (37). Thus, ER stress appears to induce $p21^{CIP1}$ expression through both p53-dependent and -independent mechanisms.

As β-cells are apparently much more sensitive to ER stress than other types of cells and tissues (39), ER stress might be a more common cause of β-cell failure than previously thought, especially in terms of the increased insulin demands of modern lifestyles. Our data indicate that both increased apoptosis and impaired proliferation, in β-cells, are mechanisms leading to β-cell loss in *wfs1*-deficient islets, a model of ER-stress mediated β-cell failure. Further studies designed to elucidate the molecular mechanisms of β-cell loss under chronic ER stress are anticipated to contribute to future treatments for type 2 diabetes.

MATERIALS AND METHODS

Antibodies

The monoclonal antibody against $P58^{IPK}$ was a generous gift from Prof. M.G. Katze (University of Washington). Other antibodies were purchased from the indicated sources: anti-GRP94, anti-KDEL (Stressgen Biotechnologies), anti-GRP78, anti-XBP1, anti-$p21^{CIP1}$, anti-CHOP, anti-p53, anti-phosphorylated p53 and anti-ATF4 (Santa Cruz Biotechnology), anti-HRD1 (Abgent), anti-phosphorylated PERK, anti-JNK, anti-phosphorylated JNK, anti-eIF2α, anti-phosphorylated eIF2α, and anti-cleaved caspase-3 (Cell Signaling), and anti-$p27^{KIP1}$ (BD Transduction Laboratories).

Mouse islet isolation, real-time RT–PCR and western blot

The *wfs1*-deficient mice used had a C57Bl/6 background and were described previously (17). All animal experiments were approved by the Tohoku University Institutional Animal Care and Use Committee (#15–45). Islets were isolated by collagenase infusion through the common bile duct and harvested by hand. Total RNA was prepared immediately after islet isolation using an RNAeasy kit (Qiagen). For real-time RT–PCR analysis, cDNA was synthesized by reverse transcription using the oligo $d(T)_{16}$ primer and subjected to PCR amplification with gene-specific primers (Table 1) using a SYBR Green 1 kit (Roche). Data are presented as relative values to actin mRNA. For detection of the spliced form of XBP1 mRNA, the primers were: 5′-TGAGAACCAGGA GTTAAGAAACGC-3′ and 5′-TTCTGGGTAGACCTCTGG GAGTTCC-3′. For immunoblotting, islets from three to four mice were pooled, dissolved immediately after isolation in a lysis buffer (~100 islets/15 μl) and subjected to SDS–polyacrylamide gel electrophoresis. In several experiments, isolated islets were cultured overnight and treated with 0.5 μM TG for 12 h. All western blot experiments were repeated at least three times, with different sets of samples, throughout this study. Immunoblot band intensities were analyzed using Scion image software (Scion Corporation) and normalized with those of actin.

Establishment of MIN6wfs1$^{-/-}$ and MIN6wfs1$^{+/-}$ cell lines

The *wfs1*$^{-/-}$ mice (17) were bred with IT6 mice expressing SV40 large T antigen under the human insulin promoter (24) and the resulting *wfs1*$^{+/-}$:SV40Tag/+ mice were further bred with *wfs1*$^{-/-}$ mice. Tumors from pancreases of 10- to 12-week-old *wfs1*$^{+/-}$:SV40Tag/+ and *wfs1*$^{-/-}$:SV40Tag/+ mice were carefully excised and placed in Dulbecco's Modified Eagle's Medium containing penicillin and streptomycin. Cells were expanded and frozen at passages 3 and 4. We used these cells at 5–8 passages in this study. For study of apoptosis, MIN6 cells were infected with AdRI-PeGFP expressing enhanced green fluorescent protein under the insulin promoter to facilitate detection of cells under fluorescent microscope. Apoptosis was examined by staining with annexin V using the Annexin V-Cy3 apoptosis detection kit

Table 1. Primers used for quantitative real-time RT–PCR

Genes	Forward	Reverse
ATF4	5′-TCCTGAACAGCGAAGTGTTG-3′	5′-ACCCATGAGGTTTCAAGTGC-3′
GRP94	5′-TGATGAAGTCGACGTGGATG-3′	5′-TCCTGTTCACTTCAGCTTGG-3′
GRP78	5′-GACATTTGCCCAGAAGAAA-3′	5′-CTCATGACATTCAGTCCAGCA-3′
P58^{IPK}	5′-CCTTATCGGACAGTCCTTCG-3′	5′-TCAGAGTCCTGATTTCATCTTCA-3′
EDEM	5′-GGAAATTCATCCGAGTTCCA-3′	5′-GGGCCATGTACAACAATTCA-3′
CHOP	5′-CCTAGCTTGGCTGACAGAGG-3′	5′-CTGCTCCTTCTCCTTCATGC-3′
GADD34	5′-CGGAGAGAAGCCAGAATCAC-3′	5′-CAGCAAGGAAATGGACTGTG-3′
P21^{CIP1}	5′-ACATCTCAGGGCCGAAAAC-3′	5′-CCTGACCCACAGCAGAAGAG-3′

(Medical and Biological Laboratories). At least 1000 cells per sample were counted for annexin V positive cells.

GRP78 promoter assay

The pGL3-promoter, pTK-RLuc and pGL3-basic plasmids were purchased from Promega. The mouse GRP78 promoter fragment spanning −172 to −21 (positions relative to the transcription start site) was amplified by PCR using oligonucleotides 5′-GACTCGAGGCCGCTTCGAATCGGCAG-3′ and 5′-TCAAGCTTGGCCAGTATCGAGCGCGC-3′. This fragment contains three ER stress response elements (40) and the corresponding regions of human (40) and rat (41) *GRP78* genes were shown to respond to ATF6 activation. A GRP78 promoter-driving luciferase reporter plasmid (designated pmGRP78pro(−172)-Luc) was constructed by subcloning this fragment into the *Xho*I and *Hind*III sites of the pGL3-basic vector. MIN6wfs1$^{+/-}$ or MIN6wfs1$^{-/-}$ cells were co-transfected with pGL3-promoter or pGRP78pro(−172)-Luc together with pTK-RLuc using the LipofectAMINE reagent (Invitrogen). Luciferase activities were assayed with Dual-Luciferase reporter system (Promega) using a Lumat LB9507 luminometer (Berthold).

BrdU incorporation assay

BrdU (100 mg/kg) was injected into the mice intraperitoneally. Six hours later, the mice were sacrificed and their pancreases were fixed with 4% paraformaldehyde. Immunohistochemical analyses were performed with a Cell Proliferation Assay kit (BD Pharmingen). Sections were also stained with anti-insulin. BrdU-positive β-cells were counted in at least 50 sections per mouse.

Recombinant adenovirus experiments

Human *GRP78* cDNA was purchased from Open Biosystems. Human *WFS1* cDNA was a generous gift from Prof. Y. Tanizawa (Yamaguchi University). The CMV promoter containing two Tet-operator sequences (designated CTO) was excised from pcDNA5/TO (Invitrogen) and ligated to these cDNAs. The Tet-repressor cDNA was excised from pcDNA6/TR (Invitrogen) and ligated to the CAG promoter unit (42). These expression units were used to generate recombinant adenoviruses by a previously described method (43). The resulting viruses were designated AdCAG-TR for the Tet-repressor expressing virus and AdCTO-GRP78 for the GRP78 expressing virus under the CTO promoter, and so on. MIN6 and its derivative cells were infected with AdCAG-TR at a multiplicity of infection (m.o.i.) of 30 together with viruses with the CTO promoter at an m.o.i. of 100. One day after infection, cells were reseeded and divided into two groups. Two days thereafter, the cells were fed media with or without doxycycline (2 μg/ml). We have observed no adverse effects of infection of a control recombinant adenovirus expressing green fluorescence protein at an m.o.i. of less than 250 on MIN6 cell function in terms of cell proliferation and glucose-stimulated insulin secretion (data not shown). For the cell number assessment, MIN6 cells infected with AdCAG-TR and AdCTO-p21^{CIP1} were seeded in six-well plates at 2×10^5 per well, cultured in media with or without doxycycline (2 μg/ml) and harvested after the indicated intervals. Cells were then stained with trypan blue and counted.

Statistical analysis

Data are presented as means ± S.E. Differences between groups were assessed by Student's *t*-test.

ACKNOWLEDGEMENTS

We thank Profs. M.G. Katze and Y. Tanizawa for their generous gifts of the monoclonal antibody against P58^{IPK} and human WFS1 cDNA, respectively. We are also grateful to Y. Nagura and K. Tanaka for their expert assistance. This research was supported by Grants-in-Aid for Scientific Research (17590264 to H.I. and 17390258 to Y.O.) from the Ministry of Education, Science, Sports and Culture of Japan.

Conflict of Interest statement. None declared.

REFERENCES

1. Donath, M.Y. and Halban, P.A. (2004) Decreased beta-cell mass in diabetes: significance, mechanisms and therapeutic implications. *Diabetologia*, **47**, 581–589.
2. Rhodes, C.J. (2005) Type 2 diabetes–a matter of beta-cell life and death? *Science*, **307**, 380–384.
3. Porter, J.R. and Barrett, T.G. (2005) Monogenic syndromes of abnormal glucose homeostasis: clinical review and relevance to the understanding of the pathology of insulin resistance and beta cell failure. *J. Med. Genet.*, **42**, 893–902.
4. Butler, A.E., Janson, J., Bonner-Weir, S., Ritzel, R., Rizza, R.A. and Butler, P.C. (2003) Beta-cell deficit and increased beta-cell apoptosis in humans with type 2 diabetes. *Diabetes*, **52**, 102–110.

5. Harding, H.P. and Ron, D. (2002) Endoplasmic reticulum stress and the development of diabetes: a review. *Diabetes*, **51** (Suppl. 3), S455–S461.
6. Wu, J. and Kaufman, R.J. (2006) From acute ER stress to physiological roles of the unfolded protein response. *Cell Death Differ.*, **13**, 374–384.
7. Schroder, M. and Kaufman, R.J. (2005) The mammalian unfolded protein response. *Annu. Rev. Biochem.*, **74**, 739–789.
8. Harding, H.P., Zhang, Y., Zeng, H., Jungries, R., Chung, P., Plesken, H., Sabatini, D.D. and Ron, D. (2001) Diabetes mellitus and exocrine pancreatic dysfunction in perk−/− mice reveals a role for translational control in secretory cell survival. *Mol. Cell*, **7**, 1153–1163.
9. Delepine, M., Nicolino, M., Barrett, T., Golamaully, M., Lathrop, G.M. and Julier, C. (2000) *EIF2AK3*, encoding translation initiation factor 2-alpha kinase 3, is mutated in patients with Wolcott-Rallison syndrome. *Nat. Genet.*, **25**, 406–409.
10. Scheuner, D., Song, B., McEwen, E., Liu, C., Laybutt, R., Gillespie, P., Saunders, T., Bonner-Weir, S. and Kaufman, R.J. (2001) Translational control is required for the unfolded protein response and *in vivo* glucose homeostasis. *Mol. Cell*, **7**, 1165–1176.
11. Ladiges, W.C., Knoblaugh, S.E., Morton, J.F., Korth, M.J., Sopher, B.L., Baskin, C.R., MacAuley, A., Goodman, A.G., LeBoeuf, R.C. and Katze, M.G. (2005) Pancreatic β-cell failure and diabetes in mice with a deletion mutation of the endoplasmic reticulum molecular chaperone gene $P58^{IPK}$. *Diabetes*, **54**, 1074–1081.
12. Wolfram, D.J. and Wagener, H.P. (1938) Diabetes mellitus and simple optic atrophy among siblings: report on four cases. *Mayo Clinic Proc.*, **13**, 715–718.
13. Inoue, H., Tanizawa, Y., Wasson, J., Behn, P., Kalidas, K., Bernal-Mizrachi, E., Mueckler, M., Marshall, H., Donis-Keller, H., Crock, P. *et al.* (1998) A gene encoding a transmembrane protein is mutated in patients with diabetes mellitus and optic atrophy (Wolfram syndrome). *Nat. Genet.*, **20**, 143–148.
14. Strom, T.M., Hortnagel, K., Hofmann, S., Gekeler, F., Scharfe, C., Rabl, W., Gerbitz, K.D. and Meitinger, T. (1998) Diabetes insipidus, diabetes mellitus, optic atrophy and deafness (DIDMOAD) caused by mutations in a novel gene (wolframin) coding for a predicted transmembrane protein. *Hum. Mol. Genet.*, **7**, 2021–2028.
15. Takeda, K., Inoue, H., Tanizawa, Y., Matsuzaki, Y., Oba, J., Watanabe, Y., Shinoda, K. and Oka, Y. (2001) *WFS1* (Wolfram syndrome 1) gene product: predominant subcellular localization to endoplasmic reticulum in cultured cells and neuronal expression in rat brain. *Hum. Mol. Genet.*, **10**, 477–484.
16. Karasik, A., O'hara, C., Srikanta, S., Swift, M., Soeldner, J.S., Kahn, C.R. and Herskowitz, R.D. (1989) Genetically programmed selective islet beta-cell loss in diabetic subjects with Wolfram's syndrome. *Diab. Care*, **12**, 135–138.
17. Ishihara, H., Takeda, S., Tamura, A., Takahashi, R., Yamaguchi, S., Takei, D., Yamada, T., Inoue, H., Soga, H., Katagiri, H. *et al.* (2004) Disruption of the *wfs1* gene in mice causes progressive beta-cell loss and impaired stimulus-secretion coupling in insulin secretion. *Hum. Mol. Genet.*, **13**, 1159–1170.
18. Yamaguchi, S., Ishihara, H., Tamura, A., Yamada, T., Takahashi, R., Takei, D., Katagiri, H. and Oka, Y. (2004) Endoplasmic reticulum stress and *N*-glycosylation modulate expression of WFS1 protein. *Biochem. Biophys. Res. Commun.*, **325**, 250–256.
19. Ueda, K., Kawano, J., Takeda, K., Yujiri, T., Tanabe, K., Anno, T., Akiyama, M., Nozaki, J., Yoshinaga, T., Koizumi, A. *et al.* (2005) Endoplasmic reticulum stress induces *Wfs1* gene expression in pancreatic β cells via transcriptional activation. *Eur. J. Endocr.*, **153**, 167–176.
20. Fonseca, S.G., Fukuma, M., Lipson, K.L., Nguyen, L.X., Allen, J.R., Oka, Y. and Urano, F. (2005) WFS1 is a novel component of the unfolded protein response and maintains homeostasis of the endoplasmic reticulum in pancreatic β-cells. *J. Biol. Chem.*, **280**, 39609–39615.
21. Riggs, A.C., Bernal-Mizrachi, E., Ohsugi, M., Wasson, J., Fatrai, S., Welling, C., Murray, J., Schmidt, R.E., Herrera, P.L. and Permutt, M.A. (2005) Mice conditionally lacking the Wolfram gene in pancreatic islet beta cells exhibit diabetes as a result of enhanced endoplasmic reticulum stress and apoptosis. *Diabetologia*, **48**, 2313–2321.
22. Kaneko, M., Ishiguro, M., Niinuma, Y., Uesugi, M. and Nomura, Y. (2002) Human HRD1 protects against ER stress-induced apoptosis through ER-associated degradation. *FEBS Lett.*, **532**, 147–152.
23. Hosokawa, N., Wada, I., Hasegawa, K., Yorihuzi, T., Tremblay, L.O., Herscovics, A. and Nagata, K. (2001) A novel ER alpha-mannosidase-like protein accelerates ER-associated degradation. *EMBO Rep.*, **2**, 415–422.
24. Miyazaki, J., Araki, K., Yamato, E., Ikegami, H., Asano, T., Shibasaki, Y., Oka, Y. and Yamamura, K. (1990) Establishment of a pancreatic β cell line that retains glucose-inducible insulin secretion: special reference to expression of glucose transporter isoforms. *Endocrinology*, **127**, 126–132.
25. Brewer, J.W. and Diehl, J.A. (2000) PERK mediates cell-cycle exit during the mammalian unfolded protein response. *Proc. Natl Acad. Sci. USA*, **97**, 12625–12630.
26. Georgia, S. and Bhushan, A. (2004) Beta cell replication is the primary mechanism for maintaining postnatal beta cell mass. *J. Clin. Invest.*, **114**, 963–968.
27. Kushner, J.A., Ciemerych, M.A., Sicinska, E., Wartschow, L.M., Teta, M., Long, S.Y., Sicinski, P. and White, M.F. (2005) Cyclins D2 and D1 are essential for postnatal pancreatic beta-cell growth. *Mol. Cell. Biol.*, **25**, 3752–3762.
28. Barone, M.V., Crozat, A., Tabaee, A., Philipson, L. and Ron, D. (1994) CHOP (GADD153) and its oncogenic variant, TLS-CHOP, have opposing effects on the induction of G1/S arrest. *Genes Dev.*, **8**, 453–464.
29. Kim, D.-G., You, K.-R., Liu, M.-J., Choi, Y.-K. and Won, Y.-S. (2002) GADD153-mediated anticancer effects of *N*-(4-hydroxyphenyl)retinamide on human hepatoma cells. *J. Biol. Chem.*, **277**, 38930–38938.
30. Marciniak, S.J., Yun, C.Y., Oyadomari, S., Novoa, I., Zhang, Y., Jungreis, R., Nagata, K., Harding, H.P. and Ron, D. (2004) CHOP induces death by promoting protein synthesis and oxidation in the stressed endoplasmic reticulum. *Genes Dev.*, **18**, 3066–3077.
31. Hollander, M.C., Poola-Kella, S. and Fornace, A.J., Jr (2003) Gadd34 functional domains involved in growth suppression and apoptosis. *Oncogene*, **22**, 3827–3832.
32. Yagi, A., Hasegawa, Y., Xiao, H., Haneda, M., Kojima, E., Nishikimi, A., Hasegawa, T., Shimokata, K. and Isobe, K. (2003) GADD34 induces p53 phosphorylation and p21/WAF1 transcription. *J. Cell. Biochem.*, **90**, 1242–1249.
33. McBain, S.C. and Morgan, N.G. (2003) Functional effects of expression of wolframin-antisense transcripts in BRIN-BD11 beta-cells. *Biochem. Biophys. Res. Commun.*, **307**, 684–688.
34. Sherr, C.J. and Roberts, J.M. (1999) CDK inhibitors: positive and negative regulators of G1-phase progression. *Genes Dev.*, **13**, 1501–1512.
35. Cozar-Castellano, I., Weinstock, M., Haughty, M., Velazquez-Garcia, S., Sipula, D. and Stewart, A.F. (2006) Evaluation of β-cell replication in mice transgenic for hepatocyte growth factor and placental lactogen. Comprehensive characterization of the G1/S regulatory proteins reveals unique involvement of $p21^{CIP1}$. *Diabetes*, **55**, 70–77.
36. Yang, L., Sara, G., Carlson, S.G., McBurney, D. and Horton, W.E., Jr (2005) Multiple signals induce endoplasmic reticulum stress in both primary and immortalized chondrocytes resulting in loss of differentiation, impaired cell growth, and apoptosis. *J. Biol. Chem.*, **280**, 31156–31165.
37. Zu, K., Bihani, T., Lin, A., Park, Y.M., Mori, K. and Ip, C. (2006) Enhanced selenium effect on growth arrest by BiP/GRP78 knockdown in p53-null human prostate cancer cells. *Oncogene*, **25**, 546–554.
38. Uchida, T., Nakamura, T., Hashimoto, N., Matsuda, T., Kotani, K., Sakaue, H., Kido, Y., Hayashi, Y., Nakayama, K.I., White, M.F. and Kasuga, M. (2005) Deletion of Cdkn1b ameliorates hyperglycemia by maintaining compensatory hyperinsulinemia in diabetic mice. *Nat. Med.*, **11**, 175–182.
39. Shi, Y., Taylor, S.I., Tan, S.L. and Sonenberg, N. (2003) When translation meets metabolism: multiple links to diabetes. *Endocr. Rev.*, **24**, 91–101.
40. Yoshida, H., Haza, K., Yanagi, H., Yura, T. and Mori, K. (1998) Identification of the *cis*-acting endoplasmic reticulum stress response element responsible for transcriptional induction of mammalian glucose-regulated proteins. *J. Biol. Chem.*, **273**, 33741–33749.
41. Lee, A.S. (2005) The ER chaperone and signaling regulator GRP78/Bip as a monitor of endoplasmic reticulum stress. *Methods*, **35**, 373–381.
42. Niwa, H., Yamamura, K. and Miyazaki, J. (1991) Efficient selection for high-expression transfectants with a novel eukaryotic vector. *Gene*, **108**, 193–199.
43. Tashiro, F., Niwa, H. and Miyazaki, J. (1999) Constructing adenoviral vectors by using the circular form of the adenoviral genome cloned in a cosmid and the Cre-loxP recombination system. *Hum. Gene Ther.*, **10**, 1845–1852.

Neuronal Pathway from the Liver Modulates Energy Expenditure and Systemic Insulin Sensitivity

Kenji Uno,[1,2*] Hideki Katagiri,[2*†] Tetsuya Yamada,[1*] Yasushi Ishigaki,[1] Takehide Ogihara,[2] Junta Imai,[1,2] Yutaka Hasegawa,[1,2] Junhong Gao,[1,2] Keizo Kaneko,[1,2] Hiroko Iwasaki,[2] Hisamitsu Ishihara,[1] Hironobu Sasano,[3] Kouichi Inukai,[4] Hiroyuki Mizuguchi,[5] Tomoichiro Asano,[6] Masakazu Shiota,[7] Masamitsu Nakazato,[8] Yoshitomo Oka[1]

Coordinated control of energy metabolism and glucose homeostasis requires communication between organs and tissues. We identified a neuronal pathway that participates in the cross talk between the liver and adipose tissue. By studying a mouse model, we showed that adenovirus-mediated expression of peroxisome proliferator–activated receptor (PPAR)–γ2 in the liver induces acute hepatic steatosis while markedly decreasing peripheral adiposity. These changes were accompanied by increased energy expenditure and improved systemic insulin sensitivity. Hepatic vagotomy and selective afferent blockage of the hepatic vagus revealed that the effects on peripheral tissues involve the afferent vagal nerve. Furthermore, an antidiabetic thiazolidinedione, a PPARγ agonist, enhanced this pathway. This neuronal pathway from the liver may function to protect against metabolic perturbation induced by excessive energy storage.

The incidence of obesity, insulin resistance, hyperlipidemia, and hypertension, collectively referred to as the metabolic syndrome, is increasing at an alarming rate in Western cultures (*1*). Secreted humoral factors, including leptin (*2*), convey information about energy storage from adipose tissue to the central nervous system (CNS). As in adipose tissues, fat storage in the liver is dynamically changed by overall energy balance, but our understanding of how the liver transmits metabolic signals to other tissues remains incomplete. Studies of mouse models created by tissue-specific genetic engineering (*3*, *4*) or adenoviral gene transfer (*5*, *6*) have shown the importance of cross talk between tissues in the regulation of energy metabolism. Mice with tissue-specific knockout of peroxisome proliferator–activated receptor γ (PPARγ) provide an example of such intertissue communication (*7*). PPARγ activates genes involved in lipid storage and metabolism (*8*). Although PPARγ expression in the liver is low compared with that in adipose tissues (*9*), hepatic expression of PPARγ (*10*, *11*), especially that of PPARγ2 (*12*), is functionally enhanced in a number of obesity models. In addition, liver-specific disruption of PPARγ in obese (ob/ob) mice prevents hepatic steatosis but increases peripheral adiposity and decreases insulin sensitivity in muscle and fat (*13*). Thus, hepatic PPARγ2 plays important roles not only in the development of liver steatosis but also in the regulation of peripheral lipid storage and insulin sensitivity.

To investigate the mechanism by which hepatic PPARγ2 expression affects metabolism in peripheral tissues, we overexpressed PPARγ2 in the livers of C57BL/6 mice using adenoviral gene transfer. After being fed a high-fat diet for 4 weeks, the mice developed obesity-associated diabetes (*14*). The PPARγ2 adenovirus vector was then administered intravenously to mice (PPARγ2 mice). Control mice given the LacZ adenovirus (LacZ mice) showed no alterations in blood glucose levels, food intake, or plasma lipid parameters after virus administration (*14*). Systemic infusion of the PPARγ2 adenovirus into mice resulted in expression of the transgene primarily in the liver (Fig. 1A), without increased expression in peripheral tissues, including white adipose tissue (WAT) (Fig. 1B).

The livers of PPARγ2 mice were pale and enlarged as compared with those of control mice (fig. S1A). Liver weights were significantly increased (Fig. 1C) because of increased triglyceride content (Fig. 1D). Histological analysis of PPARγ2 mice revealed an abundance of large lipid droplets in the livers, without apparent inflammation or structural change (fig. S1B). Thus, hepatic PPARγ2 expression induced severe hepatic steatosis. Hepatic PPARγ2 expression enhanced the expression of lipogenesis-related genes (fig. S2), suggesting that increased uptake and synthesis of fatty acids induce severe steatosis.

In contrast, WAT in PPARγ2 mice was notably diminished in size (fig. S1A); for example, epididymal fat weight was decreased by 46.6% in PPARγ2 mice versus controls (Fig. 1E). Cell diameters in WAT and brown adipose tissue (BAT) were also markedly decreased in PPARγ2 mice (fig. S1C). The increases in body weights induced by a high-fat diet were suppressed in PPARγ2 mice (Fig. 1F). Resting oxygen consumption was increased by 29.4% in PPARγ2 mice (Fig. 1G), whereas food intake did not differ from that of LacZ mice (Fig. 1H).

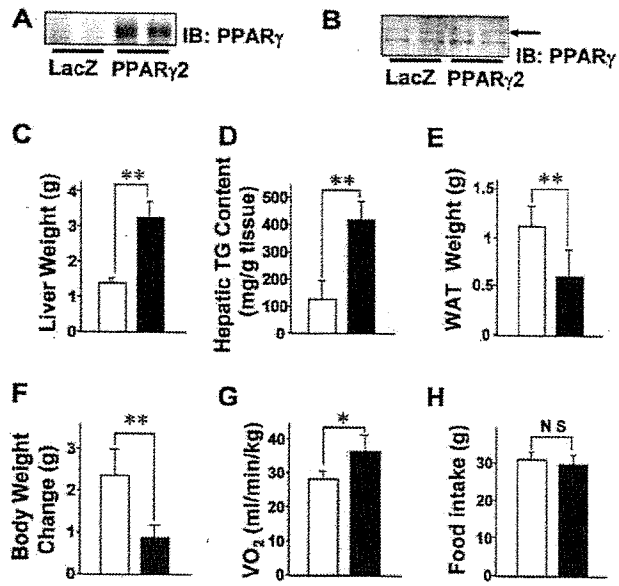

Fig. 1. Hepatic PPARγ2 expression aggravates hepatic steatosis but diminishes peripheral adiposity. (**A** and **B**) Immunoblotting (IB) with an antibody to PPARγ of liver (A) and epididymal fat (B) extracts. Liver weight (**C**), triglyceride (TG) content (**D**), and epididymal fat tissue (WAT) weights (**E**) are shown. Experiments in (A) to (E) were performed on day 7 after adenoviral administration. (**F**) Body weight changes during the 7 days after adenoviral administration. (**G**) Resting oxygen consumption (VO_2) was measured on day 3 after adenoviral injection. (**H**) Total food intake was measured for 7 days after adenoviral administration. In (C) to (H), white and black bars indicate results from LacZ mice and PPARγ2 mice, respectively. Significance as compared to LacZ mice is indicated (**$P < 0.01$ and *$P < 0.05$) by an unpaired t test. NS, not significant.

[1]Division of Molecular Metabolism and Diabetes, [2]Advanced Therapeutics for Metabolic Diseases, Center for Translational and Advanced Animal Research, [3]Department of Pathology, Tohoku University Graduate School of Medicine, Sendai 980–8575, Japan. [4]The Fourth Department of Internal Medicine, Saitama Medical School, Moroyama, Iruma-gun, Saitama 350–0495, Japan. [5]Laboratory of Gene Transfer and Regulation, National Institute of Biomedical Innovation, Osaka 567–0085, Japan. [6]Department of Physiological Chemistry and Metabolism, University of Tokyo, Tokyo 113–8655, Japan. [7]Department of Molecular Physiology and Biophysics, Vanderbilt University Medical Center, Nashville, TN 37232, USA. [8]Third Department of Internal Medicine, Miyazaki Medical College, University of Miyazaki, Kiyotake, Miyazaki 889–1692, Japan.

*These authors contributed equally to this work.
†To whom correspondence should be addressed E-mail: katagiri@mail.tains.tohoku.ac.jp

Thus, hepatic PPARγ2 expression increased systemic energy expenditure, thereby suppressing high-fat diet–induced weight gain.

Control mice were hyperglycemic, hyperinsulinemic, and hyperleptinemic in response to a 5-week-long high-fat diet. Hepatic PPARγ2 expression decreased fasting blood glucose and insulin levels (Fig. 2A), indicating markedly improved systemic insulin sensitivity. As shown in Fig. 2B, PPARγ2 mice also showed a 79% reduction in serum leptin levels. Although serum adiponectin levels were similar to those in control mice, tumor necrosis factor–α (TNF-α) levels were significantly decreased in PPARγ2 mice. These findings are consistent with a reduction in peripheral adiposity.

Glucose tolerance (Fig. 2C) and insulin tolerance (Fig. 2D) tests showed that hepatic expression of PPARγ2 markedly improved insulin sensitivity and glucose tolerance. Furthermore, improved insulin sensitivity in muscle (fig. S3A) and epididymal fat tissue (fig. S3B) was confirmed by enhanced tyrosine phosphorylation of the insulin receptor and insulin receptor substrate–1 in response to insulin administration. Thus, hepatic PPARγ2 expression clearly exerts remote beneficial effects on insulin sensitivity in muscle and WAT. Although insulin sensitivity in the liver was impaired (fig. S3C), hepatic PPARγ coactivator (PGC)–1α and hepatic phosphoenolpyruvate carboxykinase (PEPCK) expression was decreased (Fig. 2E), suggesting decreased hepatic glucose output.

To further examine insulin sensitivity and endogenous glucose production in PPARγ2 mice, we performed hyperinsulinemic euglycemic clamp experiments. Basal glucose production in PPARγ2 mice was decreased by 22% as compared with that in LacZ mice, whereas insulin's ability to suppress endogenous glucose production was severely blunted in PPARγ2 mice (Fig. 2F). In addition, glucose infusion rates in PPARγ2 mice were markedly increased (Fig. 2G). Thus, hepatic PPARγ2 expression improved insulin sensitivity in the periphery and decreased glucose output from the liver despite hepatic insulin resistance.

Serum free–fatty-acid (FFA) levels were markedly increased in PPARγ2 mice (fig. S4A), suggesting that hepatic PPARγ2 expression promotes hydrolysis of triglycerides stored in adipose tissues. Increased expression levels of the uncoupling protein (UCP)–1 (*15*), PGC1α (*16*), and hormone-sensitive lipase (*17*) in BAT (fig. S4B) and WAT (fig. S4C) indicate high tonus of the sympathetic nerves innervating these adipose tissues. In addition, the administration of bupranorol, a pan–β-adrenergic blocker (*18*), decreased serum FFA in PPARγ2 mice but had no effect in LacZ mice (fig. S4D), confirming that the β-adrenergic nerve function enhances lipolysis in adipose tissues of PPARγ2 mice.

To examine whether afferent nerves originating in the liver mediate the remote effects, we dissected the hepatic branch of the vagus nerve. Seven days after selective hepatic vagotomy (HV), we administered recombinant adenovirus encoding LacZ or PPARγ2 to mice. Hepatic PPARγ2 expression similarly altered liver weights, hepatic triglyceride content, and PEPCK expression in mice subjected to HV and sham operation (SO) (Table 1). In contrast, selective HV completely blocked the decreases in WAT weights and brown adipocyte size as well as the increases in serum FFA, resting oxygen consumption, and WAT UCP1 expression in PPARγ2 mice (Table 1), indicating that the hepatic vagus mediates the remote effects of hepatic PPARγ2 expression.

HV involves dissection of both afferent and efferent vagal branches innervating the liver. To determine whether the remote effects of hepatic PPARγ2 expression are mediated by the afferent vagus, we applied a specific afferent neurotoxin, capsaicin, to the hepatic branch of the vagus of diet-induced obese male Sprague-Dawley (SD) rats. Seven days after perivagal application of capsaicin or vehicle, we administered recombinant adenovirus encoding LacZ or PPARγ2. Expression of calcitonin gene–related peptide, a sensory neuropeptide, was markedly decreased in the capsaicin-treated vagal nerve, whereas immunoreactivity for S100 proteins was similar in vehicle- and capsaicin-treated nerves (fig. S5A). Furthermore, transmission electron microscopic analyses (fig. S5B) revealed selective degradation of unmyelinated fibers in the vagal hepatic branch. In addition, application of capsaicin to this branch did not affect the esophageal branch of the posterior vagal trunk (fig. S5). These observations indicate selective deafferentation of the hepatic branch of the vagus. Under these conditions, perivagal capsaicin treatment completely blocked the hepatic PPARγ2 expression–induced decrease in WAT weight (Table 1). When taken together, these findings strongly suggest that afferent vagal nerve ac-

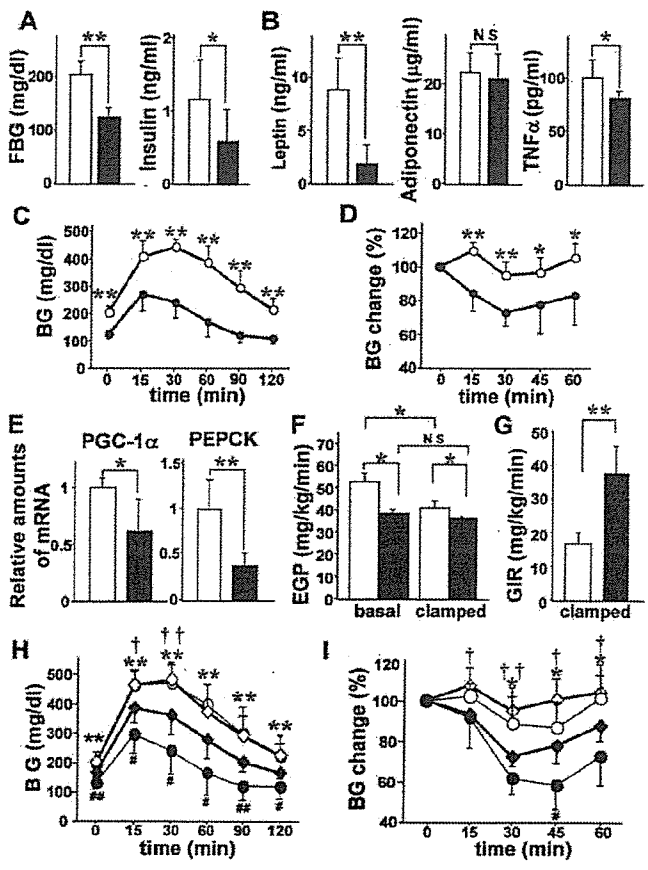

Fig. 2. Hepatic PPARγ2 expression improves peripheral insulin resistance. Fasting blood glucose (FBG) and serum insulin (**A**) and adipocytokines (**B**) were measured in LacZ mice (white bars) and PPARγ2 mice (black bars) on day 7 after adenoviral administration. These serum parameters were measured after a 10-hour fast. (**C** and **D**) LacZ mice (open circles) and PPARγ2 mice (solid circles) were subjected to glucose tolerance (C) and insulin tolerance (D) tests. BG, blood glucose. (**E**) Relative amounts of PGC-1α and PEPCK mRNA in the liver were measured by quantitative reverse transcriptase polymerase chain reaction. (**F** and **G**) Metabolic variables during hyperinsulinemic euglycemic clamp. Endogenous glucose production (EGP) in basal and clamped states (F) and rates of glucose infusion (GIR) were required to maintain euglycemia during the clamp study (G). Experiments in (A) to (G) were performed on day 7 after adenoviral administration. In (A), (B), and (E) to (G), white and black bars indicate results from LacZ mice and PPARγ2 mice, respectively. Significance as compared to LacZ mice is indicated (**$P < 0.01$ and *$P < 0.05$) by an unpaired t test. NS, not significant. (**H** and **I**) HV or SO was performed 7 days before the administration of LacZ or PPARγ2 adenovirus. Mice were subjected to glucose tolerance (H) and insulin tolerance (I) tests on day 7 after adenoviral administration. Open and solid circles indicate SO LacZ mice and SO PPARγ2 mice, respectively. Open and solid diamonds indicate HV LacZ mice and HV PPARγ2 mice, respectively. Data are presented as mean ± SD. **($P < 0.01$) and *($P < 0.05$) indicate significance in SO LacZ mice versus SO PPARγ2 mice, ††($P < 0.01$) and †($P < 0.05$) indicate significance in HV LacZ mice versus HV PPARγ2 mice, and ##($P < 0.01$) and #($P < 0.05$) indicate significance in HV PPARγ2 mice versus SO PPARγ2 mice, by unpaired t tests.

tivation originating in the liver mediates the remote effects of hepatic PPARγ2 expression on peripheral lipolysis.

We next examined the effects of HV on glucose (Fig. 2H) and insulin (Fig. 2I) tolerance test results in PPARγ2 mice. In SO mice, glucose tolerance and insulin sensitivity were improved by hepatic PPARγ2 expression, but these improvements were partially suppressed by hepatic branch vagotomy. These findings suggest that hepatic PPARγ2 expression improved glucose tolerance and systemic insulin sensitivity via both improved peripheral insulin sensitivity and decreased hepatic glucose output; the former requires afferent vagal and efferent sympathetic nerves, whereas the latter does not.

Next, to determine whether the neuronal system, consisting of afferent vagal and efferent sympathetic nerves, functions in the physiological setting of enhanced endogenous PPARγ2 expression in the liver, we examined the effects of an antidiabetic thiazolidinedione (TZD, a PPARγ agonist) using db/db mice, which are a murine model of genetic obesity and diabetes. In db/db mice, endogenous expression of PPARγ2, at both the mRNA (Fig. 3A) and the protein (fig. S6A) levels, is markedly enhanced in the liver. To eliminate the secondary effects of body weight changes, troglitazone, a TZD derivative, was given to db/db mice for 2 days, followed by an evaluation of acute effects. The TZD administration did not alter body weights (Fig. 3B) but did increase resting oxygen consumption (Fig. 3C) and UCP1 expression in BAT (Fig. 3D) and WAT (Fig. 3E), suggesting activation of sympathetic nerves to BAT and WAT. Dissection of the hepatic branch of the vagus 7 days before TZD administration reversed the increases in resting oxygen consumption (Fig. 3C) as well as UCP1 expression in BAT (Fig. 3D) and WAT (Fig. 3E). These findings indicate that the neuronal pathway originating in the liver is also involved in the acute systemic effects of TZDs, under conditions in which hepatic PPARγ expression is upregulated, such as in obese subjects.

To further examine whether endogenous PPARγ in the liver affects energy metabolism, we knocked down hepatic PPARγ in db/db mice. Administration of recombinant adenovirus expressing short hairpin RNA for PPARγ (*19*) 7 days before TZD treatment substantially decreased endogenous PPARγ expression in the liver (fig. S6B) as well as hepatic triglyceride content (fig. S6C) and sterol regulatory element binding protein–1c expression (fig. S6D), indicating functional knockdown of hepatic PPARγ (*20*). Under these conditions, TZD-enhanced energy expenditure was partially but significantly suppressed (fig. S6E). Thus, endogenous PPARγ in the liver regulates acute energy metabolism in vivo. TZD treatment reportedly alleviates insulin resistance in adipose-tissue–ablated mice (*10*) and adipose-specific-PPARγ–deficient mice (*21*), which may involve the aforementioned hepatic-PPARγ–induced neuronal activation in addition to a muscle PPARγ contribution (*22*).

We have shown that a neuronal pathway, consisting of the afferent vagus from the liver and efferent sympathetic nerves to adipose tissues, is involved in the regulation of energy expenditure, systemic insulin sensitivity, glucose metabolism, and fat distribution between the liver and the periphery. Because hepatic PPARγ expression is physiologically associated with obesity, the liver may convey information regarding excess energy balance to the CNS via the afferent vagus. This neuronal system may underlie chronic adaptive thermogenesis, resulting in protection against metabolic perturbation induced by excessive energy storage. There are two avenues of communication between the

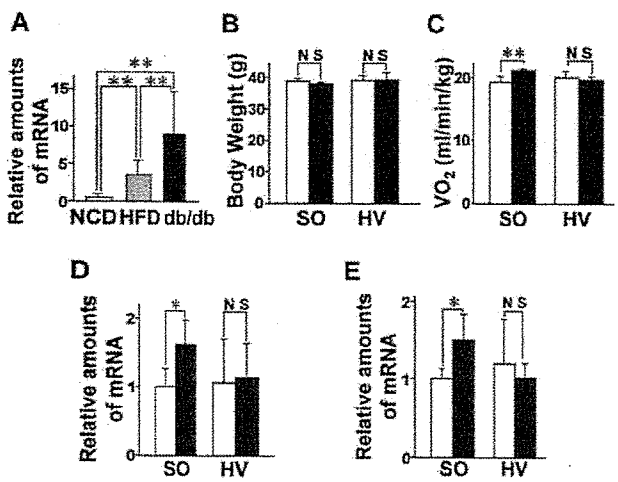

Fig. 3. HV inhibits TZD-enhanced energy expenditure in obese mice. (**A**) Relative amounts of PPARγ2 mRNA in the livers of normal chow diet–fed (NCD) C57BL/6 mice, high-fat diet–fed (HFD) C57BL/6 mice, and normal chow diet–fed db/db (db/db) mice. (**B** to **E**) db/db mice were subjected to HV or SO 7 days before the 2-day administration of TZD (black bars) or vehicle (white bars), after which body weights (B) and resting oxygen consumptions (C) were measured. Relative amounts of UCP1 mRNA in BAT (D) and epididymal fat tissue (E) from mice fed ad libitum. Data are presented as mean ± SD. Significance as compared to control mice is indicated (**$P < 0.01$ and *$P < 0.05$) by an unpaired t test. NS, not significant.

Table 1. Afferent vagal activation from the liver is involved in remote effects of hepatic PPARγ2 expression. (Upper section) Mice were subjected to HV or SO 7 days before administration of LacZ or PPARγ2 adenovirus. Resting oxygen consumption (VO_2) was measured on day 3 after adenoviral injection. Mice were killed after a 10-hour fast on day 7 after adenoviral injection. (Lower section) Male SD rats with high-fat diet–induced obesity were subjected to application of capsaicin or vehicle to the vagal hepatic branch 7 days before administration of LacZ or PPARγ2 adenovirus. Seven days after adenoviral administration, epididymal fat weights were determined. Significance as compared to LacZ mice is indicated (P values) by an unpaired t test. LW, liver weight; HTG, hepatic TG content; P, PEPCK; CD, cell diameter; NS, not significant.

	SO			HV		
	LacZ	PPARγ2	P	LacZ	PPARγ2	P
LW (g)	1.11 ± 0.13	2.30 ± 0.39	<0.001	1.12 ± 0.07	2.07 ± 0.32	<0.001
HTG (mg/g tissue)	78.71 ± 46.50	171.26 ± 43.90	0.008	62.02 ± 24.92	215.09 ± 75.78	<0.001
P mRNA (liver)	1.00 ± 0.21	0.50 ± 0.17	0.003	1.356 ± 0.460	0.54 ± 0.22	0.002
WAT weight (g)	1.13 ± 0.13	0.85 ± 0.14	<0.001	1.04 ± 0.26	1.06 ± 0.19	NS
BAT CD (μm)	11.55 ± 4.45	7.69 ± 2.09	<0.001	10.63 ± 3.38	10.55 ± 3.93	NS
FFA (μEq/l)	556.14 ± 87.33	860.47 ± 206.04	0.005	533.14 ± 59.50	558.38 ± 151.58	NS
VO_2 (ml/min/kg)	30.25 ± 2.38	34.38 ± 3.03	0.015	32.73 ± 4.54	31.98 ± 4.05	NS
UCP1 mRNA (WAT)	1.00 ± 0.24	2.36 ± 0.77	0.019	2.05 ± 0.64	1.82 ± 1.15	NS
	Vehicle			**Capsaicin**		
WAT weight (g)	8.95 ± 0.99	7.06 ± 1.32	0.024	8.70 ± 1.14	8.85 ± 1.71	NS

brain and other tissues: humoral factors and neuronal pathways. Leptin, a humoral factor from adipocytes, is a mediator of metabolic information from adipose tissue to the hypothalamus (*2*). In addition, circulating nutrients reportedly affect food intake and alter hepatic glucose production via the efferent vagal pathway (*23*, *24*). An afferent vagal signal originating in the liver is likely to be another metabolic information pathway. In this way, the brain may integrate information obtained from several tissues and organs via both humoral and neuronal pathways. When the brain receives information regarding excess energy storage, the sympathetic nervous system is activated to enhance energy expenditure and lipolysis, thereby maintaining energy homeostasis. Disturbance of the control system is implicated in the development of the metabolic syndrome (*25*). Targeting of this neuronal pathway is a potential therapeutic strategy for treating the metabolic syndrome.

References and Notes

1. J. S. Flier, *Cell* **116**, 337 (2004).
2. J. M. Friedman, J. L. Halaas, *Nature* **395**, 763 (1998).
3. Y. Minokoshi, C. R. Kahn, B. B. Kahn, *J. Biol. Chem.* **278**, 33609 (2003).
4. T. Kitamura, C. R. Kahn, D. Accili, *Annu. Rev. Physiol.* **65**, 313 (2003).
5. J. An *et al.*, *Nat. Med.* **10**, 268 (2004).
6. T. Yamada *et al.*, *Cell Metab.* **3**, 223 (2006).
7. O. Gavrilova *et al.*, *J. Biol. Chem.* **278**, 34268 (2003).
8. V. Bocher, I. Pineda-Torra, J. C. Fruchart, B. Staels, *Ann. N.Y. Acad. Sci.* **967**, 7 (2002).
9. L. Fajas *et al.*, *J. Biol. Chem.* **272**, 18779 (1997).
10. C. F. Burant *et al.*, *J. Clin. Invest.* **100**, 2900 (1997).
11. L. Chao *et al.*, *J. Clin. Invest.* **106**, 1221 (2000).
12. R. Rahimian *et al.*, *Mol. Cell. Biochem.* **224**, 29 (2001).
13. K. Matsusue *et al.*, *J. Clin. Invest.* **111**, 737 (2003).
14. Y. Ishigaki *et al.*, *Diabetes* **54**, 322 (2005).
15. I. Nagase *et al.*, *J. Clin. Invest.* **97**, 2898 (1996).
16. J. Gomez-Ambrosi, G. Fruhbeck, J. A. Martinez, *Mol. Cell. Endocrinol.* **176**, 85 (2001).
17. Y. Hatakeyama, Y. Sakata, S. Takakura, T. Manda, S. Mutoh, *Am. J. Physiol. Regul. Integr. Comp. Physiol.* **287**, R336 (2004).
18. A. Wellstein, D. Palm, G. G. Belz, *J. Cardiovasc. Pharmacol.* **8** (suppl. 11), S36 (1986).
19. T. Hosono *et al.*, *Gene* **348**, 157 (2005).
20. S. Herzig *et al.*, *Nature* **426**, 190 (2003).
21. W. He *et al.*, *Proc. Natl. Acad. Sci. U.S.A.* **100**, 15712 (2003).
22. A. L. Hevener *et al.*, *Nat. Med.* **9**, 1491 (2003).
23. A. Pocai, S. Obici, G. J. Schwartz, L. Rossetti, *Cell Metab.* **1**, 53 (2005).
24. T. K. Lam *et al.*, *Nat. Med.* **11**, 320 (2005).
25. M. W. Schwartz, D. Porte Jr., *Science* **307**, 375 (2005).

26. We thank M. Kaji, T. Takai, Y. Sato, H. Yawo, T. Hashikawa, M. Kanzaki, Y. Minokoshi, and M. Tominaga for advice and discussions. Supported by grants-in-aid from the Ministry of Education, Science, Sports, and Culture of Japan (H.K.), a grant-in-aid from the Ministry of Health, Labor, and Welfare of Japan (Y.O.), and the 21st Century Center of Excellence Programs (H.K. and Y.O.).

Supporting Online Material

www.sciencemag.org/cgi/content/full/312/5780/1656/DC1
Materials and Methods
SOM Text
Figs. S1 to S6
Table S1
References

9 February 2006; accepted 8 May 2006
10.1126/science.1126010

Synaptic Amplifier of Inflammatory Pain in the Spinal Dorsal Horn

Hiroshi Ikeda,* Johanna Stark, Harald Fischer, Matthias Wagner, Ruth Drdla, Tino Jäger, Jürgen Sandkühler†

Inflammation and trauma lead to enhanced pain sensitivity (hyperalgesia), which is in part due to altered sensory processing in the spinal cord. The synaptic hypothesis of hyperalgesia, which postulates that hyperalgesia is induced by the activity-dependent long-term potentiation (LTP) in the spinal cord, has been challenged, because in previous studies of pain pathways, LTP was experimentally induced by nerve stimulation at high frequencies (~100 hertz). This does not, however, resemble the real low-frequency afferent barrage that occurs during inflammation. We identified a synaptic amplifier at the origin of an ascending pain pathway that is switched-on by low-level activity in nociceptive nerve fibers. This model integrates known signal transduction pathways of hyperalgesia without contradiction.

Inflammation of peripheral tissues causes spontaneous pain and hyperalgesia. Amplification of pain-related information in the spinal dorsal horn lamina I contributes to inflammatory pain (*1*–*6*). Inflammation causes release of neuromodulators, including substance P and glutamate in spinal dorsal horn (*7*, *8*), potentially leading to Ca^{2+}-dependent LTP. In all previous studies, spinal LTP was induced by brief (1 s), high-frequency (100 Hz) burstlike stimulation (HFS) of afferent nerve fibers. High-frequency bursts do not, however, resemble the continuous low-frequency afferent barrage that occurs during inflammation. Low-frequency presynaptic activity normally fails to induce LTP but rather induces synaptic long-term depression (LTD) (*9*). The LTP model of inflammatory hyperalgesia thus may be questioned. Here, we evaluated the effect of low-frequency afferent barrage on synaptic transmission in ascending pain pathways and asked if synaptic plasticity is differentially induced in distinct ascending pain tracts. We labeled lamina I projection neurons by retrograde fluorescent marker DiI (1,1′-dioctadecyl-3,3,3′,3′-tetramethylindocarbocyanine perchlorate), injected into either of two major projection areas of spinal lamina I neurons: the parabrachial (PB) area or the periaqueductal gray (PAG) (*10*, *11*) (Fig. 1, A and B). To circumvent confounding developmental factors, we used only juvenile or adult rats in this study. Transverse spinal cord slices with long dorsal roots attached were prepared 3 to 4 days after DiI injections to allow whole-cell recordings from identified projection neurons in 21- to 28-day-old rats (*10*). In the presence of tetrodotoxin, bath application of substance P (2 μM) induced transient inward currents in 21 out of 27 spino-PB and in 9 out of 12 spino-PAG neurons (Fig. 1C), confirming the expression of functional neurokinin 1 receptors (NK1Rs). Spinal release of substance P following electrical stimulation of primary afferents at C-fiber strength was assessed by the internalization of NK1R in lamina I neurons. HFS parameters (100-Hz bursts) similar to all previously used conditioning stimulation protocols to induce classical LTP in pain pathways, or low-frequency stimulation (LFS, 2 Hz), was used. Both types of stimulation elicited substantial NK1R internalization in 89 ± 1% and in 78 ± 4% of 150 neurons evaluated in three rats per group (Fig. 1D). We then used these stimulation protocols for conditioning.

Conditioning HFS induces LTP at synapses between C-fibers and lamina I neurons that project to the PB (*12*). We confirmed these results by showing LTP of monosynaptically evoked excitatory postsynaptic currents (EPSCs) to 172 ± 15% of the control value at 30 min after conditioning (n = 8) (Fig. 2A). However, conditioning electrical stimulation within the typical frequency band of C-fibers during inflammation (2 Hz) (*13*) did not change synaptic strength in any of the spino-PB neurons tested (108 ± 19% of control, n = 7) (Fig. 2C). LFS, however, did modify synaptic strength in spinal lamina I neurons with a projection to the PAG. In all spino-PAG neurons tested, LFS induced a robust LTP of monosynaptic C-fiber–evoked EPSCs [to 262 ± 30% of the control value at 30 min after stimulation (n = 18) and to 346 ± 33% at 60 min (n = 8)] (Fig. 2D). In all seven lamina I neurons with a projection to the PAG, conditioning stimulation at high frequency was ineffective (98 ± 10%, n = 7) (Fig. 2B). Monosynaptic, A-fiber–evoked

Department of Neurophysiology, Center for Brain Research, Medical University of Vienna, Vienna, Austria.

*Present address: Department of Human and Artificial Intelligence Systems, University of Fukui, 3-9-1 Bunkyo, Fukui 910-8507, Japan.

†To whom correspondence should be addressed. E-mail: juergen.sandkuehler@meduniwien.ac.at

Cold Exposure Suppresses Serum Adiponectin Levels through Sympathetic Nerve Activation in Mice

Junta Imai,†‡¶ Hideki Katagiri,†‡¶ Tetsuya Yamada,*¶ Yasushi Ishigaki,* Takehide Ogihara,† Kenji Uno,*† Yutaka Hasegawa,*† Junhong Gao,*†‡ Hisamitsu Ishihara,* Hironobu Sasano,§ and Yoshitomo Oka**

Abstract

IMAI, JUNTA, HIDEKI KATAGIRI, TETSUYA YAMADA, YASUSHI ISHIGAKI, TAKEHIDE OGIHARA, KENJI UNO, YUTAKA HASEGAWA, JUNHONG GAO, HISAMITSU ISHIHARA, HIRONOBU SASANO, AND YOSHITOMO OKA. Cold exposure suppresses serum adiponectin levels through sympathetic nerve activation in mice. *Obesity*, 2006;14:1132–1141.

Objective: Several lines of evidence suggest important roles for adiponectin in glucose and lipid metabolism and atherosclerosis. However, the mechanisms regulating serum adiponectin levels and adiponectin production are still not completely understood. Our aim was to determine whether adiponectin synthesis is physiologically regulated by the sympathetic nervous system (SNS).

Research Methods and Procedures: Mice were exposed to cold (4 °C) for 12 hours and for 24 hours with or without inhibition of noradrenaline synthesis or pan-β adrenergic function, followed by measurement of serum adiponectin concentrations and levels of adiponectin and uncoupling protein (UCP) 1 expressions in various white adipose tissues (WATs).

Results: Cold exposure significantly reduced serum adiponectin concentrations without changing body weights or WAT sizes in either subcutaneous or intra-abdominal fat tissues. The serum adiponectin reduction was associated with a decrease in adiponectin mRNA expression in subcutaneous, epididymal, and mesenteric fat tissues. In these adipose tissues, UCP1 expression was markedly enhanced, suggesting SNS activation in these tissues. Administration of α-methyl-*p*-tyrosine or a combination of SR59230A and propranolol reversed the cold-exposure–induced decreases in serum adiponectin concentrations and adiponectin mRNA expression in these tissues. In contrast, in retroperitoneal fat, the effects of cold exposure on adiponectin and UCP1 expressions were strikingly weak but were not reversed by SNS inhibitors.

Discussion: SNS physiologically regulates serum adiponectin levels and adiponectin synthesis in WATs in vivo, although responsiveness to SNS stimulation differs markedly among WATs. Sympathetic activation might be involved in development of the metabolic syndrome by modulation of serum adiponectin concentrations.

Key words: white adipose tissue, adipocytokine, α-methyl-*p*-tyrosine, SR59230A, metabolic syndrome

Introduction

Obesity results from disruption of the balance between caloric intake and energy expenditure and is associated with insulin resistance (1). Insulin resistance is a fundamental contributor to the metabolic syndrome associated with type 2 diabetes, hypertension, hyperlipidemia, and atherosclerosis. Among the major advancements in this field were the discoveries of adipocyte-derived factors, such as leptin, adiponectin, free fatty acids (2), tumor necrosis factor-α (3), and plasminogen-activator inhibitor-1 (4). These adipocyte-derived factors play crucial roles in insulin sensitivity. Free fatty acids, tumor necrosis factor-α, and plasminogen-activator inhibitor-1 reportedly contribute to development of insulin resistance in vivo and in vitro (2–4), whereas adiponectin increases insulin sensitivity.

Received for review April 8, 2005.
Accepted in final form April 5, 2006.
The costs of publication of this article were defrayed, in part, by the payment of page charges. This article must, therefore, be hereby marked "advertisement" in accordance with 18 U.S.C. Section 1734 solely to indicate this fact.
Divisions of *Molecular Metabolism and Diabetes and †Advanced Therapeutics for Metabolic Diseases, Center for Translational and Advanced Animal Research, ‡Tohoku University 21st Century COE Program "Comprehensive Research and Education Center for Planning of Drug Development and Clinical Evaluation," and §Department of Pathology, Tohoku University Graduate School of Medicine, Sendai, Japan.
¶ These authors contributed equally to the paper.
Address correspondence to Hideki Katagiri, Division of Advanced Therapeutics for Metabolic Diseases, Center for Translational and Advanced Animal Research, Tohoku University Graduate School of Medicine, 2-1 Seiryo-machi, Aoba-ku, Sendai 980-8575, Japan.
E-mail: katagiri@mail.tains.tohoku.ac.jp

Adiponectin was originally identified as a protein induced during adipogenesis (5–8). Low serum adiponectin levels were demonstrated in murine models of obesity and insulin resistance (6). In humans, serum adiponectin levels are inversely correlated with body weights and adiposity (9–11), suggesting important roles of adiponectin in the development of insulin resistance in obese subjects. In addition, adiponectin is reportedly involved in protection against atherosclerosis (12–14). Low serum levels of adiponectin are associated with atherogenesis in obese and insulin-resistant subjects (15,16). Therefore, to understand the pathophysiology of metabolic syndrome associated with insulin resistance and to develop novel therapeutic targets for the metabolic syndrome, it is essential to elucidate the mechanisms regulating adiponectin production and the resultant serum adiponectin levels.

There is considerable evidence that leptin is regulated by many types of stimuli (17–21). Notably, the sympathetic nervous system (SNS)[1] reportedly regulates leptin synthesis both in vitro and in vivo. In isolated brown and white adipocytes, leptin synthesis is suppressed by β3 adrenergic receptor (AR) agonists (18). In addition, SNS stimulation by acute cold exposure decreases leptin mRNA in white and brown adipose tissues (BATs) (22,23). Blockade of noradrenaline synthesis by α-methyl-*p*-tyrosine (α-MPT) causes marked increases in leptin mRNA in white adipose tissue (WAT) and plasma leptin levels (24). Thus, SNS activation suppresses leptin synthesis, thereby decreasing serum leptin in vivo.

In contrast, SNS involvement in adiponectin regulation is somewhat controversial. In 3T3-L1 adipocytes, isoproterenol, a β-adrenergic stimulant, reportedly reduced adiponectin mRNA, and this inhibitory effect was reversed by pretreatment with propranolol, a β-adrenergic antagonist (25). In mice, administration of a β-adrenergic stimulant reduced adiponectin mRNA expression in adipose tissue and serum adiponectin concentrations (26), suggesting SNS involvement in adiponectin regulation in vivo. However, Puerta et al. (22) reported that cold-exposure (18 hours at 6 °C)–induced SNS activation did not significantly affect adiponectin expression in WAT or the serum adiponectin concentrations in rats, although adiponectin mRNA levels were reduced in BAT. Conversely, cold exposure (24 hours at 4 °C) also reportedly increases serum adiponectin levels (27). Thus, the physiological role of SNS in adiponectin regulation is unclear and remains controversial. Therefore, to determine whether SNS is involved in physiological regulation of adiponectin synthesis in vivo, we exposed mice to cold environments with or without inhibition of noradrenaline synthesis or pan-β adrenergic function. To achieve inhibition of noradrenaline synthesis and β adrenergic function, mice were treated with α-MPT and a combination of SR59230A and propranolol, a β3 AR antagonist and a β1/β2 AR antagonist, respectively. We then examined the effects of these treatments on adiponectin expression in various WATs and on serum adiponectin concentrations. Herein, we report that, although the degrees of effects differed among WATs, cold exposure decreased adiponectin expression in subcutaneous, epididymal, and mesenteric fat tissues, resulting in significantly decreased serum adiponectin concentrations. Furthermore, the effects of cold exposure were suppressed by inhibition of noradrenaline synthesis or β adrenergic function. To our knowledge, this is the first study demonstrating that SNS activation physiologically influences serum adiponectin concentrations in vivo.

[1] Nonstandard abbreviations: SNS, sympathetic nervous system; AR, adrenergic receptor; BAT, brown adipose tissue; α-MPT, α-methyl-*p*-tyrosine; WAT, white adipose tissue; UCP, uncoupling protein; SE, standard error; PPAR, peroxisome proliferator activator.

Research Methods and Procedures

Animals

Animal studies were conducted under protocols in accordance with the institutional guidelines for animal experiments at Tohoku University. Ten-week-old male C57BL/6N mice were purchased from Clea (Tokyo, Japan), housed in an air-conditioned environment, with a 12-hour light-dark cycle, and fed a regular unrestricted diet. Mice were divided into two body-weight–matched groups; mice in the cold-stimulated group were placed in a cold room (4 °C) for 12 hours or for 24 hours with the same light-dark schedule as control mice, whereas for the control group, the temperature was 25 °C. In several experiments, 150 mg/kg body weight α-MPT (Sigma, St. Louis, MO) was intraperitoneally injected immediately before the exposure to 4 °C or 25 °C. In several other experiments, a combination of 1.5 mg/kg body weight SR59230A (Sigma) and 1.5 mg/kg body weight (*S*)-(−)-propranolol (Sigma) was intraperitoneally injected immediately before starting the experiment and then every 4 hours for the 24-hour duration of exposure to 4 °C or 25 °C. Body weights were measured before and after cold exposure. Food intake amounts during these periods were also determined. Blood samples were obtained before and immediately after cold exposure. The mice were then sacrificed and epididymal fat, subcutaneous fat, mesenteric fat, and retroperitoneal fat were rapidly removed, immediately frozen in liquid N_2, and stored at −80 °C until analysis.

Histological Analysis

Each adipose tissue was stained with hematoxylin and eosin. Total adipocyte areas were traced manually and analyzed. Cell diameters were measured for 100 or more adipocytes in each group.

Immunoassay

Serum adiponectin concentrations were measured using a mouse/rat adiponectin ELISA Kit (Otsuka Pharmacy, To-